Collective Features in Polyisobutylene. A Study of the Static and Dynamic Structure Factor by Molecular Dynamics Simulations

Y. Khairy,[†] F. Alvarez,[†,‡] A. Arbe,[*,†] and J. Colmenero[†,‡,¶]

Centro de Física de Materiales (CSIC–UPV/EHU) – Materials Physics Center (MPC), Paseo Manuel de Lardizabal 5, 20018 San Sebastián, Spain, Departamento de Física de Materiales (UPV/EHU), Apartado 1072, 20080 San Sebastián, Spain, and Donostia International Physics Center, Paseo Manuel de Lardizabal 4, 20018 San Sebastián, Spain

E-mail: a.arbe@ehu.es

[*]To whom correspondence should be addressed

[†]Centro de Física de Materiales (CSIC–UPV/EHU) – Materials Physics Center (MPC), Paseo Manuel de Lardizabal 5, 20018 San Sebastián, Spain

[‡]Departamento de Física de Materiales (UPV/EHU), Apartado 1072, 20080 San Sebastián, Spain

[¶]Donostia International Physics Center, Paseo Manuel de Lardizabal 4, 20018 San Sebastián, Spain

Abstract

We present a study of the static and dynamic structure factor of polyisobutylene (PIB) by fully atomistic molecular dynamics simulations. The reliability of the simulated cell is first assured by computing the magnitudes measured by diffraction and neutron spin echo techniques on a fully deuterated sample and directly comparing the results with those previously obtained from experiments [B. Farago et al., *Phys. Rev. E* **2002**, *65*, 051803]. Taking advantage of the validated simulations, we have disentangled the contributions to the static and dynamic structure factor by using a suitable grouping of the partial correlation functions based on specific molecular groups in PIB: main-chain (MC) atoms and methyl-group (MG) atoms. Regarding the structural features, we can attribute the temperature dependence of the first structure factor peak –which is dominated by inter-chain correlations mainly from backbone atoms– predominantly to the evolution of the MC/MG cross-correlations. Paradoxically, in the momentum transfer region where the MG/MG correlations present their main peak, the total structure factor displays a minimum due to a strong negative feature of the MC/MG cross-correlations. Concerning the dynamics, the decay of the intra-molecular correlations takes place through highly correlated motions relating pairs of MGs and MG and MC atoms. At inter-molecular level, the difference between pair and self-correlations for MC atoms is enhanced as the system approaches the glass-transition, indicating a gradual increase of collectivity. This collectivity of the backbones is ultimately the responsible for the modulation of the activation energy with the structure factor found in the experiments and reproduced by the simulations. Finally, we analyze the contributions of the analytical ansatz recently proposed to describe the collective relaxation time [J. Colmenero et al., *J. Chem. Phys.* **2013**, *139*, 044906] in order to identify the key ingredient leading to the above mentioned modulation of the activation energy, which is successfully accounted for by the model.

INTRODUCTION

The access to collective features through the application of neutron scattering techniques to deuterated materials, in particular polymers, offers a great deal of valuable information on the structural and dynamical properties of these systems. Considering fully deuterated samples, the short-range order is manifested by the presence of peaks (broadened in the case of amorphous systems) in the diffraction results in the momentum transfer (Q)-range above $\approx$ 0.5 Å^{-1}; furthermore, the evolution of the structure factor through the molecular dynamics is directly accessible by quasielastic neutron scattering. Despite the power of this kind of experiments, due to the complexity inherent to systems like glass-forming polymers, the interpretation of the results is not always straightforward. Regarding the structural properties, only in the case of main-chain polymers like 1,4-polybutadiene (1,4-PB) a clear assignment of the diffraction peaks is possible based exclusively on experimental results as function of temperature. As it was nicely shown in Ref.,[1] the static structure factor $S(Q)$ of 1,4-PB displays a main peak centered at about 1.48 Å^{-1} which origin can be attributed to inter-molecular correlations between nearest neighboring chains and a second broader peak at about 2.7 Å^{-1} which has to be of intra-molecular nature. Once the identity of the peaks is unveiled, dynamical measurements can be used to characterize the processes giving rise to the decay of the corresponding correlations. In the particular case of 1,4-PB, measurements of the normalized dynamic structure factor $S(Q,t)/S(Q)$ at the first peak revealed the genuine α-relaxation leading to the decorrelation of the system at inter-molecular level[2] while at the second peak provided microscopic insight on secondary relaxations related to intra-molecular motions.[3] Such kind of 'simple' phenomenological analyses are however impossible in systems with more complex chemical structure including side groups. Then, additional peaks may appear in the diffraction patterns (see, e. g.[4–7]) which origin is not necessarily related to a particular atomic pair correlation function. Of course, the ignorance of the nature of the contributing correlations to the coherent scattering completely hampers any trustable interpretation of the dynamic processes governing its time-evolution.

From an experimental point of view, polyisobutylene (PIB, -[CH_2-$C(CH_3)_2$]-$_n$) is a very thor-

oughly investigated polymer by diverse techniques including spectroscopic techniques[8–11] as well as scattering methods.[12–29] In particular, its collective features have been deeply investigated by neutron diffraction and the neutron spin echo (NSE) technique.[15,20] Despite having two methyl groups in its monomer, the static structure factor of PIB shows qualitatively the same appearance as that of 1,4-PB, i. e., without any particular signature of the presence of these side-groups. Assuming an analogous scenario as for 1,4-PB,[3] the NSE results in Ref.[15] were interpreted in terms of the merging of the α and β-relaxations, the latter being characterized as a local process involving atomic jumps over distances of about 0.5–0.9 Å. This motional amplitude was however significantly smaller than that deduced in a later work on the self-motions of PIB.[14] To rationalize these discrepancies, the authors suggested the possibility of a strong coupling between the rotation of the two methyl groups linked to the same carbon and the local backbone motions. This means, the situation seems to be much more complex than in main-chain polymers like 1,4-PB.

Furthermore, in the NSE work of Ref.,[20] the dynamic structure factor of PIB was thoroughly studied in a wide Q-range covering the region around the first structure factor peak Q_I ($Q_I \approx 1$ Å^{-1}). Surprisingly, not only the collective time but also the associated activation energy revealed a peak at about Q_I. Until now, no successful explanation of such a finding has been provided. Moreover, that work was pioneer in accessing the so-called intermediate length scales of a polymer. Intermediate scales means the region of lengths larger than inter-molecular distances ($Q \leq 0.4-0.5$ Å^{-1} approximately) but smaller than the hydrodynamic range. There, the collective characteristic time of PIB develops some kind of plateau –even suggesting the possibility of another maximum at lower Q-values around 0.3 Å^{-1}– that cannot be expected from any de Gennes-like narrowing picture.

During the last years, the development of fully atomistic molecular dynamics (MD) simulations and computer capabilities has facilitated unveiling the short-range order and shed light on the dynamical features of several glass-forming polymers (see, e. g.[30] and references therein). In particular, the combination of neutron scattering methods and MD-simulations has proved to be a highly successful tool.[30] The key of such a methodology is to use neutron scattering experiments

to validate a simulated system and thereafter obtain information from the latter that can be used to interpret the experimental results, or to calculate magnitudes that are not accessible from the experiments. Following this strategy, here we present fully atomistic MD-simulations on PIB that, once their reliability is assured, are exploited to contribute to understand the collective features of this polymer. These aspects were not considered in previous works on PIB by atomistic simulations.[31–33] We note that, unfortunately, the intermediate length/Q regime is even a more difficult range for computer simulations than for neutron scattering. The reason is very simple. In order to calculate coherent scattering at low Q-values of the order of 0.1–0.2 Å^{-1} for a cubic simulated cell, the size of this cell has to be rather large (more than 100 Å side), containing thereby a huge number of atoms. Moreover, for the low-Q values, there are only very few reciprocal vectors complying with the restrictions imposed by the size of the cell. Usually this leads to unsatisfactory statistics in the case of the calculated collective scattering function. Therefore, the characterization of the dynamic structure factor in the intermediate length scales regime is actually not possible. With the large cell simulated in this work (16840 atoms, $\approx$ 54 Å side) the Q-range available for collective correlation functions becomes effectively restricted to $Q \geq 0.6$ Å^{-1} approximately. Nevertheless, the information included in the simulations can be of utmost help to contribute to this question, as it has been shown by us in a recent paper.[34] In that work, we could reproduce the experimentally observed behavior of the collective relaxation time of PIB in the whole Q-range explored[20] applying an ansatz based on a model previously proposed by Novikov et al.[35] To do this, we made use of information provided by the present simulations –the experimentally unaccessible total self-correlation function–, and could even reproduce the intriguing feature of the modulation of the activation energy with $S(Q)$ around its first peak. However, in that paper the contributions to the collective response were not analyzed separately and the actual origin of such an effect was not discussed in depth. Here we also tackle these questions.

With these ideas in mind, the present work has been structured as follows:

- We first describe the simulation details and validate the simulated cell of PIB by direct comparison with already published neutron scattering results on coherent scattering.[20] The good

agreement allows us to further exploit the capabilities of the simulations as detailed in the following sections.

- We unveil the short-range order of PIB and disentangle the origin of its static structure factor. To do this, we have used a suitable grouping of the partial correlation functions based on specific molecular groups in the repeating unit of PIB: main-chain atoms and methyl-group atoms. In addition, the radial distribution functions have been studied in real space, separating their inter- and intra-molecular contributions.

- The dynamic structure factor is examined and compared with its self counterpart, determining the Q-range where collectivity effects are observed. They turn out to extend up to very high Q-values. To explain this behavior we have analyzed separately the partial structure factors and discussed their relative contributions to the total dynamic structure factor. Thereafter, the temperature dependence of the partial structure factors and their degree of collectivity are examined in order to explain the origin of the modulation of the activation energy on the basis of this polymer-specific information.

- Thereafter, we briefly describe the model proposed in Ref.[34] to give account for the collective relaxation in the region of the first amorphous halo and at intermediate length scales. We analyze its contributions and identify the key ingredient in this analytical model which leads to the predicted Q-dependence of the activation energy.

- We finally summarize the conclusions in a last section, where the similarities with the collectivity effects observed in other polymers are also briefly discussed.

MOLECULAR DYNAMICS SIMULATIONS

Simulation Details

Fully atomistic molecular dynamics simulations were carried out using the COMPASS forcefield implemented within the commercial software package MATERIALS STUDIO 5.0.1.[36] The COMPASS forcefield functional forms are characterized by two different kind of functions: the valence terms, which include diagonal and off-diagonal cross-coupling terms, and the nonbond interaction terms. The valence terms represent internal coordinates of bond, angle, torsion angle and out-of-plane angle, the cross-coupling terms include combinations of two or three internal coordinates. The nonbond interactions include a Lennard-Jones 9-6 function for the Van der Waals terms and a Coulombic function for electrostatic interactions. Details of the analytical expression of the functional form are given in Refs.[37–39]

The initial configuration of the simulated system was built by means of the MATERIALS STUDIO 5.1 Amorphous Cell builder.[40–42] A cubic cell containing 20 PIB chains of 70 monomers (M_w = 3922 g/mol, i. e., smaller than the entanglement mass $M_e \approx 7000$ g/mol,[43] and a total number of atoms N = 16840) was constructed at a rather high temperature of $500\,K$ (experimental $T_g \sim 200\,K$), under periodic boundary conditions. By means of NPT dynamic runs (i. e., keeping constant the number of atoms, pressure and temperature) a value of the density of $\rho = 0.8109\,g/cc$ was determined. This value is in excellent agreement with the literature data $\rho_{exp} = 0.8102\,g/cc$.[44] Such a density leads to a cell dimension of $54.12\,$Å for the cubic side. In order to minimize the obtained energy structure, the Polak-Ribiere conjugated gradients method was used. After the minimization, the system was dynamically equilibrated by a successive NVT run (i. e., keeping constant the number of atoms, volume and temperature) of $1\,ns$. The system obtained in such way was used as a starting point for collecting data every $0.01\,ps$ during a run of $1\,ns$. The production simulations were carried out in the NVT ensemble and the velocity-Verlet algorithm with a time step of $1\,fs$ was used as the integration method. To control the temperature, instead of a real temperature-bath coupling (Nose-Hoover or Berendsen thermostat) a velocity scaling procedure

with a wide temperature window of $10\,K$ was followed. Under these conditions, greater temperature fluctuations are allowed but the trajectory is disturbed less. It has been checked that, by following this simple procedure in similar polymeric systems, the results are similar to those obtained with an NVE ensemble (where the number of atoms, volume and energy are kept constant), which has the proper Newtonian dynamics.[5] After the first $1\,ns$ run, successive runs of $20\,ns$ collecting data every $0.5\,ps$ were carried out in order to reach a $100\,ns$ long dynamics. This cell was used to yield simulated systems at the lower temperatures of 470, 390, 365, 335 and 320 K. The new cells were obtained scaling the temperature and then were equilibrated running three dynamics of $1\,ns$. Once the equilibrium density was reached for each temperature, the same protocol of the first simulated sample was followed to carry out a $100\,ns$ dynamics. The densities of the equilibrated cells were found to be $\rho(470\ K) = 0.8264\,g/cc$, $\rho(390\ K) = 0.8688\,g/cc$, $\rho(365\ K) = 0.8820\,g/cc$, $\rho(335\ K) = 0.8977\,g/cc$ and $\rho(320\ K) = 0.9055\,g/cc$.

Correlation Functions and Neutron Scattering Observables

From the atomic trajectories recorded at different times it is possible to calculate different atomic correlations in the sample cell. For example, the pair correlation functions $g_{\alpha\beta}(r,t)$ can be obtained as:

$$g_{\alpha\beta}(r,t) = \frac{1}{N}\langle \sum_{i\alpha,j\beta}^{N_\alpha N_\beta} \delta(r - |\vec{r}_{i\alpha}(t) - \vec{r}_{j\beta}(0)|)\rangle. \tag{1}$$

Here the subscripts α and β refer to specific kinds of atoms (e.g., main-chain carbons, methyl-group hydrogens, etc.). In the above equation, $\vec{r}_{i\alpha}(t)$ is the position vector of the i^{th} atom of kind α at time t, and N_α, N_β are the total number of atoms of kind α and β in the sample cell. The sum runs over all the different atoms of kind α and β. The average is performed over a large number of frames to get the proper averages. The static case $t = 0$ corresponds to the radial pair probability distribution function.

The results will be partially discussed in the reciprocal space through the structure factors. The Fourier transform of $g_{\alpha\beta}(r,t)$ yields the pair correlation functions $a_{\alpha\beta}(Q,t)$ in Q-space, i. e.,

$$a_{\alpha\beta}(Q,t) = \int_0^\infty 4\pi r^2 g_{\alpha\beta}(r,t)\frac{sin(Qr)}{Qr}dr \tag{2}$$

assuming an isotropic system.

The van Hove formalism allows expressing the magnitudes experimentally accessed by neutron scattering in terms of the above correlation functions, providing thereby a unique tool to validate the simulation cell (see, e. g.[30]). The coherently scattered neutron intensity is obtained by adding up all the contributing correlations in the system properly weighted with the scattering lengths of the involved isotopes $\overline{b}_\alpha$, $\overline{b}_\beta$:[45]

$$I_{coh}(Q,t) = \sum_{\alpha,\beta} \overline{b}_\alpha \overline{b}_\beta a_{\alpha\beta}(Q,t) = \sum_{\alpha,\beta} A_{\alpha\beta}(Q,t). \tag{3}$$

Here we have introduced the correlation functions $A_{\alpha\beta}(Q,t)$, where each atomic pair correlation has been weighed with its corresponding scattering lengths. The values of the coherent scattering lengths of the isotopes composing deuterated PIB are $\overline{b}_C$ = 6.648 fm and $\overline{b}_D$ = 6.6674 fm. Due to their almost identical values, the coherently scattered intensity is very close to the true dynamic structure factor $S(Q,t)$ (all atoms equally weighted); in a diffraction experiment addressing differential cross sections, this corresponds to the true static structure factor $S(Q)$. For this reason, we will extend the use of the terms $S(Q,t)$ [$S(Q)$] to denote the function expressed by eq. 3 [eq. 3 for t = 0] when results on a fully deuterated sample are considered. The self-part of the dynamic structure factor is the result of eq. 3 when restricting the sum in eq. 1 to the terms $i\alpha = j\beta$, normalized to its static value. In an analogous way the self-counterparts of the correlation functions $A_{\alpha\beta}(Q,t)$ can be calculated. From an experimental point of view, the self-terms weighed by the corresponding incoherent scattering lengths b_α^{inc} (b_D^{inc} = 4.04 fm, b_C^{inc} = 0) determine the incoherently scattered intensity $I_{inc}(Q,t)$. In a fully deuterated sample, the incoherent contribution to the scattered intensity is much weaker than the coherent one.

Finally we note that, as follows from Eq. 2, the magnitudes measured by neutron scattering in the reciprocal space are calculated in this work by means of a Fourier transform of the corresponding van Hove correlation functions in the real space. This procedure has some advantages with respect to a direct calculation of $S(Q)$ $[S(Q,t)]$ in the reciprocal space. For instance, these magnitudes can be calculated for a larger set of Q-values, assuming isotropic systems. However, the Fourier transform method obviously has also some limitations due to the finite size of the simulation cell. These limitations mainly affect the low-Q regime, where unphysical undulations with wavelength of $4\pi/L$ (L being the side of the cubic cell) can emerge, reflecting that the van Hove correlation function can be larger or smaller than 1 for $r \rightarrow r_{max} = L/2$. In order to minimize this problem, we have restricted the low-Q range to be considered to values of Q significantly larger than the 'natural limit' of the MD-simulations defined by the size of the cell: $Q_{min} = 4\pi/L$. We have estimated our safe low-Q limit to be $Q \approx 0.6$ Å^{-1}, significantly higher than $4\pi/L \approx 0.23$ Å^{-1} ($L \approx 52$ Å). In the regime $Q \geq 0.6$ Å^{-1}, the uncertainties in the magnitudes calculated in the reciprocal space due to the Fourier transform limitations are strongly reduced and the corresponding error bars can be similar or even lower than those typical of experimental measurements (see, e. g., Figure 1). It is obvious that limiting the Q-values explored to $Q \geq 0.6$ Å^{-1} we are also minimizing the statistical errors associated to the small number of spatial configurations during the simulation runs of 100 ns in the low-temperature and low-Q regimes. Moreover, in order to reduce the statistical uncertainties at long times, the magnitudes have only be calculated up to 20 ns, eventhough the dynamic runs were extended until 100 ns.

Validation of the Simulated Cell

The validation of the dynamical aspects of the simulated cell has been performed by direct comparison with reported[20] experimental neutron spin echo (NSE) results on a fully deuterated sample. NSE experiments[46] access the normalized function

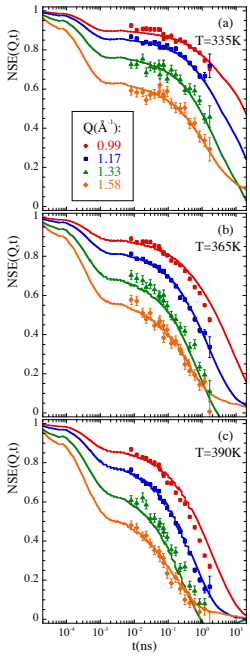

Figure 1: Comparison of the neutron spin echo results obtained from measurements on a fully deuterated PIB sample[20] (symbols) and calculated from the simulations (lines) at 335 K (a), 365 K (b) and 390 K (c) at the Q-values indicated in (a).

$$NSE(Q,t) = \frac{I_{coh}(Q,t) - \frac{1}{3}I_{inc}(Q,t)}{I_{coh}(Q,0) - \frac{1}{3}I_{inc}(Q,0)} \tag{4}$$

which for fully deuterated samples, to a good approximation, can be identified with the normalized dynamic structure factor $S(Q,t)/S(Q)$. To validate our cell we have computed from the atomic trajectories the whole function measured by this technique (Eq. 4) and directly compared simulated and experimental results. Bandpass corrections have been applied to the experimental data (see, e. g.[47]). The value considered for the band pass time was 0.2 ps. Figure 1 shows the results for selected Q-values at the three temperatures experimentally investigated. The agreement is excellent. Similar agreement is found for the other available data.

We have also analyzed the simulated NSE results (Eq. 4) at the same temperatures explored experimentally and in the NSE window investigated in Ref.[20] by using the same functional form

employed in that work. This was a stretched exponential or Kohlrausch-Williams-Watts function

$$NSE(Q,t) \approx \frac{S(Q,t)}{S(Q)} = A(Q,T)\exp\left[-\left(\frac{t}{\tau_w(Q,T)}\right)^{\beta}\right] \quad (5)$$

with free prefactor $A(Q,T)$ giving account for the decay of the correlation function at microscopic times (below ≈ 2 ps) and a fixed value of 0.55 for the stretching exponent β. The fits of the simulated data deliver characteristic times $\tau_w(Q,T)$ with the Q-dependent activation energy represented as empty circles in Figure 2. Though the values obtained from the simulations are slightly smaller than the experimental ones, they reproduce very well the experimental behavior, in particular the intriguing Q-dependence found. We have also shown that this feature is not a consequence of the remaining incoherent contribution in the NSE results (see Supplementary Information).

Thanks to the polarization analysis involved in the technique, from the NSE measurements the coherent and incoherent contributions to the differential cross section can be determined and thus the structure factor $S(Q)$ free from incoherent scattering is delivered. This magnitude provides valuable information to check the reliability of the simulated cell regarding the structural properties (short-range order). We note however that the momentum transfer range covered in those experiments is quite narrow. Therefore, we have also considered diffraction results on the same samples carried out with a triple-axis spectrometer without polarization analysis.[15,20] Figure 3 shows with filled symbols the triple-axis results at 320 K –the highest available temperature– corrected for incoherent contributions and rescaled to absolute units by using the information of the NSE results at the closest temperature (335 K, open symbols). In the same figure, the solid line represents the structure factor calculated from the simulations at 320 K. Again a remarkable agreement is found.

Furthermore, we have also compared the temperature dependence of the structure factor of simulated and real samples. In Figure 4(b) we can see that the main effect of increasing the temperature above the glass-transition in the case of the real sample is to increase the intensity in the Q-region below ≈ 1 Å^{-1}. This leads to a shift of the position of the main peak toward lower Q-values. This is exactly the behavior displayed by the simulated structure factor, as can be

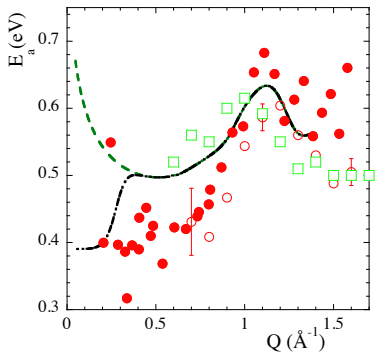

Figure 2: Momentum transfer dependence of the apparent activation energy of the characteristic time for collective relaxation obtained from KWW fits with $\beta = 0.55$ of the experimental data from Ref.[20] (solid circles) and of the full NSE function obtained from the simulations in the same temperature range and time window accessed experimentally (empty circles). For three representative Q-values the estimated error bars are shown. Empty squares show the results when variable β-values are considered to describe the simulated dynamic structure factor in the whole T-range investigated. The dashed line has been calculated on the basis of Eq. 9 by using the simulation results. Dashed-dotted line is the result of the full model proposed in Ref.[34] to describe the behavior in the intermediate length scales regime.

appreciated in Figure 4(a).

STATIC STRUCTURE FACTOR

As can be seen in Figure 3 and Figure 4 the static structure factor of PIB presents a clear main peak at $Q_I \approx 1$ Å^{-1}. A deep minimum at 1.5...1.6 Å^{-1} separates such peak from a very broad feature at higher Qs. There, two broad peaks could be resolved, centered at about 2.2 and 3 Å^{-1}. As above commented, the intensity in the low-Q flank of the main peak strongly increases with temperature leading to a shift of its position, while no appreciable T-changes are found for the

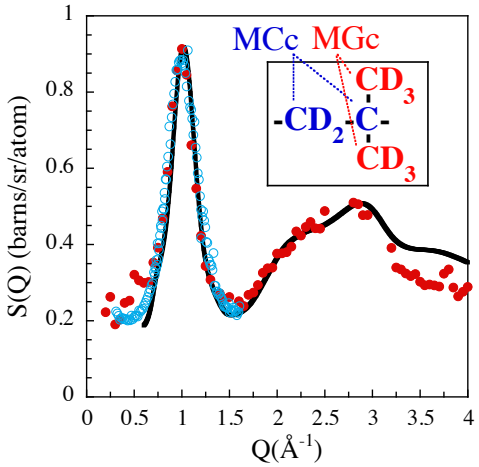

Figure 3: Comparison of the static structure factor of PIB experimentally determined on a perdeuterated sample by triple-axis (filled circles) at 320 K[20] and NSE (empty circles) at 335 K[20] and computed (line) at 320 K. The triple-axis data of Ref.[20] have been corrected to match the NSE results. The inset shows the scheme of the monomer illustrating the nomenclature used: main-chain (MC) atoms are represented in blue and methyl-group (MG) atoms in red.

broad peaks at higher Q-values. From this phenomenological observation we could conclude that the first peak is of predominantly inter-molecular origin. Applying the Bragg law its position would reveal an average inter-chain distance of $d_{chain} = 2\pi/Q_I \approx 6$ Å. On the contrary, the correlations giving rise to the features of $S(Q)$ at higher Q-values would be of intra-molecular origin (governed by covalently bonded atomic pairs). A further unbiased interpretation is not possible without an additional source of information. Let's see how the simulations can contribute to a deeper understanding of the structural features of PIB at these length scales.

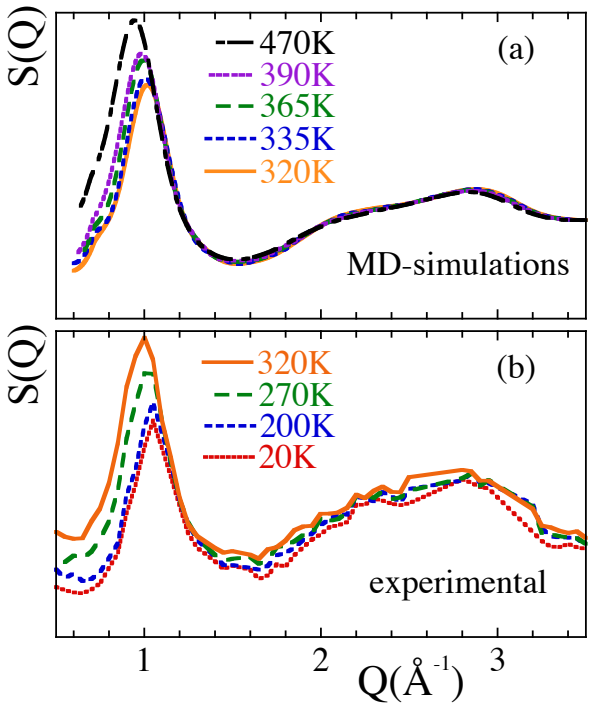

Figure 4: Temperature dependence of the static structure factor: (a) Triple-axis results[20] at different temperatures in the range $2 \leq T \leq 320$ K; (b) MD-simulations results in the investigated range.

Decomposition of $S(Q)$ in partial structure factors

We have first calculated the contributions of the two different relevant molecular groups to the static structure factor: the group of the main chain (MC) atoms which contains the two backbone carbons and the corresponding two deuterons, and the methyl groups (MG) (see inset in Figure 3). With this grouping, we have two partial correlation functions involving correlations among the atoms belonging to the same group, namely MC/MC (the contribution arising from main chain) and MG/MG (that arising from the methyl group). This grouping also leads to a cross-correlation term relating atoms from one group with atoms from other groups (MC/MG). We first focus on

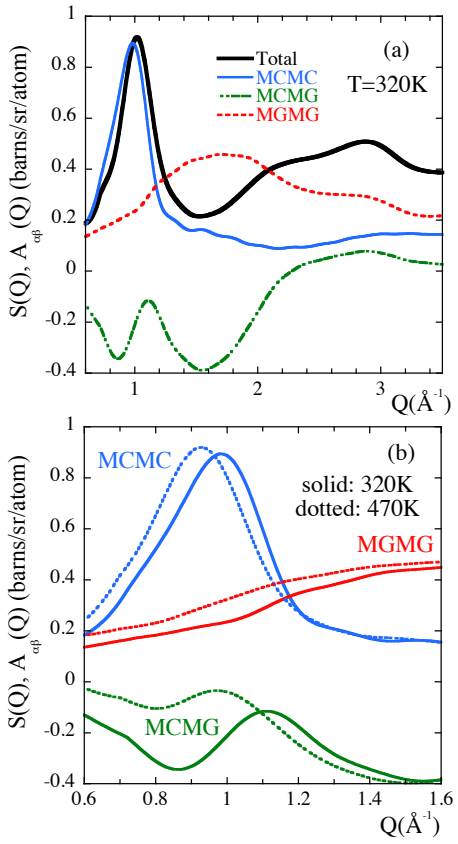

Figure 5: (a) Contributions to the static structure factor calculated from the simulations at 320 K. In (b) these contributions at 320 K (solid lines) are compared with the equivalent results at 470 K (dotted lines) in the Q-range below 1.6 Å^{-1}.

the lowest temperature considered, 320 K. Figure 5(a) shows the three partial correlation functions $A_{\alpha\beta}(Q)$ ($\alpha,\beta \in \{MC, MG\}$) contributing to the structure factor measured by neutron scattering [$S(Q)$, black line] at this temperature. For obtaining these functions, each atomic pair correlation has been weighted with its corresponding scattering lengths (eq. 3). They display the following features:

$A_{MCMC}(Q)$ shows a very pronounced peak in the same region as the main peak of the total structure factor Q_I, a shoulder at about 1.5 Å^{-1} and a very broad and weak peak around $\approx$ 3 Å^{-1}.

$A_{MGMG}(Q)$ is characterized by a main broad peak centered at about 1.6 Å^{-1} –where $S(Q)$

presents the minimum– with a shoulder at lower Q-values, in the region of Q_I. A peak around 3 Å^{-1} is also distinguishable.

$A_{MCMG}(Q)$ displays a main negative peak mirroring the main peak of A_{MGMG} at 1.6 Å^{-1}. At lower Qs, a negative peak at $\approx$ 0.85 Å^{-1} (i. e., in the region immediately below Q_I) is present which intensity is lower but comparable to that of the main peak at 1.6 Å^{-1}. Negative values of the cross-correlation function are indicative for anticorrelations between main-chain and methyl-group subsystems. At higher Q-values, a positive broad peak can be seen around 3 Å^{-1}.

Figure 5(b) compares the results corresponding to the lowest and highest temperatures investigated for $Q \leq 1.6$ Å^{-1}. With increasing temperature we observe a shift of the main peaks of the three partial correlation functions toward lower Q-values. However, the most remarkable effect is the strong weakening of the first negative peak of the cross-correlations. At Q-values above 1.6 Å^{-1} no difference is found for the structure factors at the different temperatures.

Real space analysis

In a second step we have investigated the radial distribution functions in real space. There we have distinguished inter- and intra-chain contributions. The inter-chain contributions have been obtained by considering correlations among atoms of different chains, while the intra-chain contributions arise from atoms belonging to the same chain. Figure 6 shows the results obtained at an intermediate temperature (365 K) for selected representative atoms in the system: the main-chain carbons (MCc) and the methyl-group carbons (MGc) (see inset in Figure 3).

The intra-chain contributions of the main-chain carbons [Figure 6(a)] display a sequence of well defined peaks only at quite short distances below $r \approx 5$ Å. The first peak at $r = 1.54$ Å corresponds to the covalently bonded first carbon neighbor. The second peak centered at $r = 2.6$ Å arises from second neighbors and is splitted, reflecting the bimodal distribution of bond angles in the main chain. This distribution shows two maxima centered at about 124°, corresponding to the C-CH_2-C angle, and at about 110°, corresponding to the CH_2-C-CH_2 angle.[48,49] The peaks related to the third neighbor are also very well developed: the one centered at r = 3.4 Å results from trans-

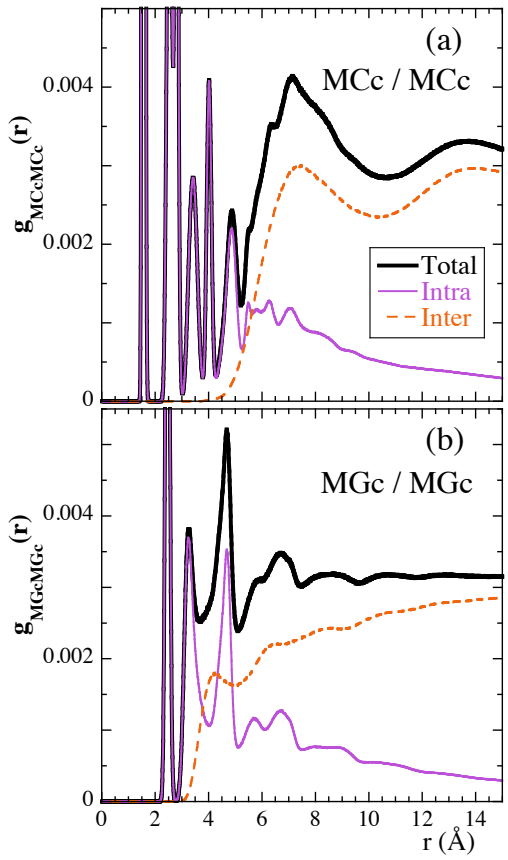

Figure 6: Radial pair correlation function calculated at 365 K, relating (a) main-chain carbons MCc and (b) methyl-group carbons MGc. The dashed lines show the inter-chain correlations, the solid lines the intra-chain correlations and thick solid lines the total functions.

gauche (t,g) conformations while the next peak at $r = 3.9$ Å arises from the all-trans state (t,t). From the peak areas the probabilities for the two conformations can be evaluated. They are 47% for trans and 53% for gauche. These populations are in agreement with the rotational isomeric state model calculations by DeBolt and Suter for PIB.[50] This finding also points to a moderate stiffness of PIB, as it is also deduced from the calculation of the characteristic ratio $C_n = \langle R_e^2 \rangle / (nb^2)$ from the simulated cell ($\langle R_e^2 \rangle$: average of the squared end-to-end vector distance, n: number of C-C bonds along the main chain, $b = 1.54$ Å: C-C bond length). We obtain $C_{140} = 5.5 \pm 0.5$, in good agreement with the experimental value of $C_\infty = 6.7$ reported for this polymer in the literature.[51] Such

flexibility explains the fast smearing of the further intra-molecular peaks at distances above 5 Å. The still clear peak at 4.8 Å is mainly due to methylene carbon correlations every two monomers. At large distances ($r > 6$ Å), the inter-chain contributions start to be more important than those of intra-molecular origin. We note that MCc atoms of different chains do not approach each other closer than about 5–6 Å. The inter-chain contribution of the correlation function $g_{MCcMCc}(r)$ displays a first peak at about 7.5 Å at 365 K. This peak position roughly corresponds to the average inter-chain distance as estimated from the main peak of the MC/MC correlations in the Q-space, $A_{MCMC}(Q)$, by means of the Bragg approximation (6.54 Å for this temperature). We can also see a second peak of this inter-chain contribution centered at about 14 Å. This peak would correspond to second-neighboring chains. Inspecting further distances, a third smooth and very broad peak located at about 21 Å can be envisaged, where a third chain would most probably be found. Thus, the value obtained from the Bragg approximation for the average inter-chain distance corresponds rather well to the observed period in the modulation of the density due to inter-chain correlations. A predominantly inter-chain origin has to be assigned to the first peak of $A_{MCMC}(Q)$ revealing such correlations. Conversely, the shoulder at about 1.5 Å^{-1} in $A_{MCMC}(Q)$ corresponding to characteristic lengths of about 4 Å must relate to intra-chain correlations (the inter-molecular contribution vanishes below 5 Å). The same applies to the peak at about 3 Å^{-1} with an equivalent distance of about 2 Å. These two peaks have to be related with the undulations of the intra-chain correlation function, that show a much shorter period in space than that of the inter-chain correlations.

Moving to the methyl-group carbons [Figure 6(b)], the intra-molecular contributions to $g_{MGcMGc}(r)$ show a first prominent peak at r = 2.5 Å. This peak contains contributions from MGcs of the same monomer and also from MGcs of consecutive monomers at the same side of the backbone, related both through (t,t) and (t,g) conformations. The next peak at r = 3.2 Å arises from MGcs at either sides of the backbone in (t,t) conformation and to the closest carbons at either sides of the backbone in (t,g) conformation. The furthest MGc atoms in (t,g) conformation give rise to the peak at r = 4.7 Å. The latter two peaks span in the region from 3 to 5 Å. At distances between 5 and 7 Å two much weaker peaks appear; the same feature could be envisaged between about 7 and 9 Å, and

also between about 9 and 11 Å. This periodicity of about 2 Å in the intra-molecular correlations between methyl group carbons would be reflected by the peak at 3 $Å^{-1}$ in $A_{MGMG}(Q)$. Conversely, the inter-chain contribution to $g_{MGcMGc}(r)$ shows a first correlation distance of about 4.2 Å which coincides with the van der Waals distance for the methane molecule:[52] methyl groups from different chains can come very close to each other. An interesting observation is the clear oscillatory feature displayed by the inter-molecular contribution of $g_{MGcMGc}(r)$ with the same period as above commented for the intra-molecular part. The maxima of the inter-molecular contribution appear at distances corresponding to the minima between the pairs of the intra-molecular peaks, giving rise to an almost constant value of the total $g_{MGcMGc}(r)$ from about 6 Å. Such a highly compact structure shall be the responsible of the low gas permeability exhibited by this polymer.[53] We note however that the minimum possible distance between main-chain carbons of 5 Å implies that there is no interpenetration of methyl groups of different chains. At about $r \geq 5$ Å the contributions to $g_{MGcMGc}(r)$ are predominantly of inter-molecular origin. From this inspection, we can deduce that the main peak of $A_{MGMG}(Q)$ at about 1.6 $Å^{-1}$ (equivalent distance of about 4 Å) has both inter- and intra-molecular origins, while the low-Q contribution is expected to be mainly of inter-molecular character.

Figure 7 compares the inter-molecular contribution to the different radial pair correlation functions relating main-chain and methyl-group carbons at the lowest and highest temperatures investigated. Let us focus first on 320 K. The function displaying non-negligible values at shorter distances is $g^{inter}_{MGcMGc}(r)$, with the already commented peak at $\approx$ 4 Å. At somewhat larger distances, the function $g^{inter}_{MCcMGc}(r)$ relating MGcs and MCcs displays a first peak corresponding to first neighbors of different chains located at $r = 6$ Å. This is a shorter distance than that characterizing next MCc neighbors of different chains. Thus, different chains approach each other at most through their methyl groups, and a main chain carbon of a given chain can come closer to a methyl group of another chain than to the backbone atoms. Consequently, the inter-molecular correlations of the MG/MG and MC/MG contributions to the structure factor extend toward larger Q-values than those of the MC/MC contribution. Conversely, we observe that the overall behavior

of $g^{inter}_{MCcMGc}(r)$ is similar to that of $g^{inter}_{MCcMCc}(r)$, but the oscillations are less well defined, indicating more distributed distances. The undulations of methyl-group correlations of inter-molecular origin show a smaller period, as above discussed.

The effects of increasing the temperature on the radial distribution functions are the following: (i) a decrease of the asymptotic value $r \rightarrow \infty$ due to the decrease of the density; (ii) a shift of the peak positions toward longer distances, reflecting the thermal expansion and (iii) a smearing of the undulations, indicating a homogeneization of the local density. In particular, the short-distance peak of $g^{inter}_{MGcMGc}(r)$ at $r \approx 4$ Å is smeared out. That of $g^{inter}_{MCcMGc}(r)$ also disappears. Also worthy of remark is the very smooth feature of $g^{inter}_{MCcMGc}(r)$: at 470 K the undulations following those of $g^{inter}_{MCcMCc}(r)$ are extremely weak. This shall be the reason of the weakening of the first negative peak of $A_{MCMG}(Q)$.

Interpretation of the features of $S(Q)$

From the above discussion we obtain a full picture of the origin of $S(Q)$ of PIB:

(i) The main peak is dominated by inter-chain correlations, mainly from backbone atoms. However, its position and intensity are strongly determined by the negative peak of the cross-correlations between main chains and methyl groups. The first-neighbor inter-molecular correlations between methyl-group atoms and between atoms from a methyl group and a main chain –which reveal a high compactness– are smeared out when the temperature increases. This leads to a smoother and broader feature of $A_{MGMG}(Q)$ and strongly reduces the (negative) contribution of $A_{MCMG}(Q)$ at low Q-values, producing an effective increase of the intensity in the region of the peak and low-Q flank of the first peak of $S(Q)$. Thus, the increase of the intensity of this main peak should not be interpreted as a signature of the enhancement of ordering in the system but contrarily as a consequence of the homogenization of the local density fluctuations. We also point out that using the shift of the main peak to monitor the dilatation of inter-chain distances leads to a somewhat larger value for the expansion coefficient than considering the bare peak from $A_{MCMC}(Q)$. The values deduced for the average inter-chain distances are also slightly different. For example,

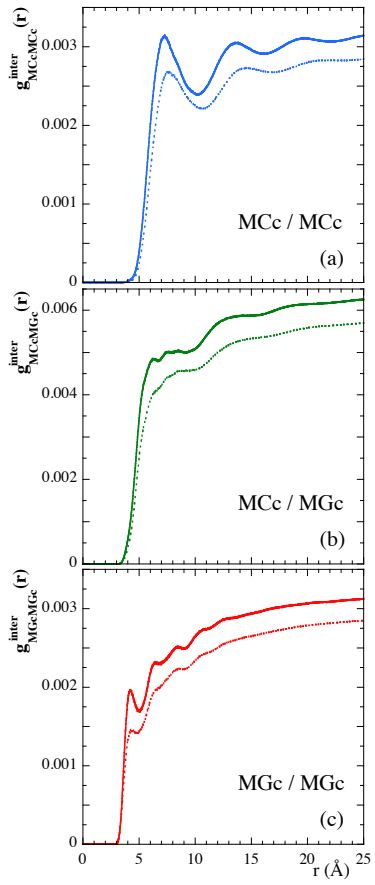

Figure 7: Inter-chain contributions to radial pair correlations relating carbons in the main chain (a), in the main chain and in the methyl group (b) and in methyl groups (c) at two different temperatures: 320 K (solid lines) and 470 K (dotted lines).

at 320 K from $S(Q)$ a value of 6.2 Å is obtained while from $A_{MCMC}(Q)$ this distance is deduced to be 6.4 Å.

(ii) The first minimum of $S(Q)$ at 1.5 Å^{-1} arises as consequence of the strong anticorrelation between main chains and methyl groups. In fact, this Q-range is where the MG/MG correlations display their main peak, and the MC/MC correlations a shoulder. We emphasize the predominantly intra-molecular character of the correlations in this region –though there is also an inter-molecular contribution from MG/MG correlations.

(iii) The peak at $Q \approx 3$ Å^{-1} reveals intra-molecular correlations of all the atoms. The in-

phase modulation of the cross-correlations with the MG/MG structure factor results from the direct association of MGs and MCs. Finally, the peak at 2.2 Å^{-1} should also be attributed to intra-chain correlations, but is not directly related to any particular peak of the partial structure factors. It appears in the Q-range where the cross-terms change sign.

We suggest the generality of the conclusions regarding the influence of cross-correlations on the first peak of $S(Q)$ for polymers with side groups. An extreme case is e. g. the family of poly(alkylene oxides), where the first peak of $S(Q)$ containing correlations of inter-backbone origin displays a very different shift with temperature from that expected from macroscopic measurements –much weaker in that case–, presumably also due to the complex interplay of the different correlations contributing to this peak.[54] Such a universality is also supported by molecular dynamics simulations results on a generic bead-spring model of comb-like polymers.[55] We finally note the strong similarity of the correlation function $A_{MCMC}(Q)$ for different polymers with side groups, like poly(methyl methacrylate) (PMMA),[6] poly(vinyl acetate) (PVAc),[7]poly(ethylene propylene) (PEP)[56] and poly(vinyl pyrrolidone) (PVP).[57] The origin of the first peak, shoulder at $Q \approx 1.5$ Å^{-1} and the peak at 3 Å^{-1} would be the same for all these polymers. In main-chain polymers like 1,4-polybutadiene (PB) or polyethylene (PE) the first peak of $S(Q)$ is located in the same region of the intra-molecular shoulder at 1.5 Å^{-1}. Therefore, the correlations there have to be partially of intra-chain origin.[58] The inter/intra contributions are the better resolved in the peaks the larger is the average inter-chain distance –i.e., in the presence of bulkier side-groups.

DYNAMIC STRUCTURE FACTOR

The quality of the simulated $S(Q,t)$ data and the wide time region over which they expand allow an accurate determination of the shape parameter for the slow decay, which unfortunately is not possible from the experimental data. Thus the $S(Q,t)/S(Q)$ data above 2 ps were described by means of Eq. 5 allowing the three parameters [A, τ_w and β] to float. The shape parameter β shows a kind of modulation with $S(Q)$ and a tendency to increase with increasing temperature

(see Figure 8(a)). We note that the value considered for β in the experiments (β = 0.55) is a good approximation of the value here found in the neighborhood of Q_I, though at lower Q-values a more markedly stretched functional form is observed from the simulations. We note that even for Q-values different from Q_I it is possible to reasonably describe the simulated results imposing the β-value used in the experimental work if the analysis is restricted to the dynamic window explored by NSE. However, the description is deficient if the whole time-range accessed by the simulations is considered. Given the change of β with Q and temperature, in the following we will discuss the results corresponding to the characteristic times in terms of the average characteristic times $\langle\tau\rangle$, that in the case of KWW functions are related with the τ_w through the expression $\langle\tau\rangle = \Gamma(1/\beta)\tau_w/\beta$. They are presented in Figure 8(b). They also show maxima at Q-values in the region around the first structure factor peak Q_I.

The degree of collectivity of the dynamics can be measured by the differences between $S(Q,t)/S(Q)$ and its self counterpart $F_s(Q,t)$. The latter function is not experimentally accessible –the incoherent scattering cross section of carbon nuclei is 0– but can be easily computed from the simulations. Figure 9 compares for the temperature of 365 K the characteristic times of the slow decay of the simulated $S(Q,t)/S(Q)$ (empty squares) and $F_s(Q,t)$ (empty circles). Interestingly enough, they differ in the whole Q-range investigated, indicating that collective effects are evident up to very high Q-values ($Q \approx 3$ Å^{-1}). Unravelling the partial contributions to $S(Q,t)/S(Q)$ and analyzing them separately is the key to unveil the origin of this collectivity.

Partial Contributions to the Dynamic Structure Factor

We consider again 365 K as a representative temperature to discuss this point. The long-time decay of the normalized total $[S(Q,t)/S(Q)]$ and partial $[A_{\alpha\beta}(Q,t)/S(Q)]$ dynamic structure factors at this temperature have been analyzed in terms of KWW functions. The values of the shape parameter and average characteristic time are displayed in Figure 10(a) and (b). We may distinguish three different Q-regions: (i) in the high-Q regime ($\approx Q \geq 1.3$ Å^{-1}) the functional form and characteristic time of all partial correlation functions roughly coincide. Thus there is a complete coupling

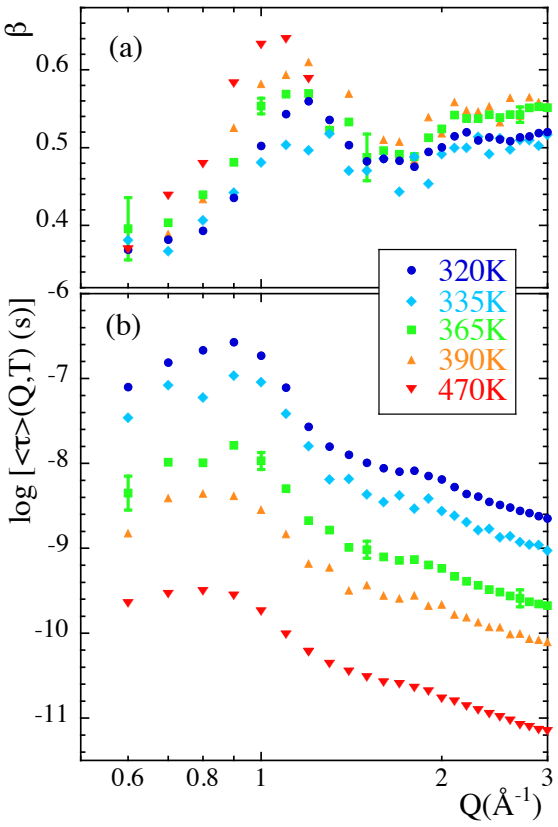

Figure 8: Momentum transfer dependence of the shape parameter (a) and average characteristic time (b) obtained from KWW fits to the dynamic structure factor at the different temperatures temperatures investigated. For 365 K and four representative Q-values the estimated error bars are shown.

between the dynamical processes governing the decay of MC/MC correlations and those relaxing the MG/MG correlations. We note that this is the region where the correlations are of basically purely intra-molecular origin. (ii) In the region $\approx 1.0 \leq Q \leq 1.3$ Å^{-1} –where inter-chain correlations start to contribute– the MC/MC correlations become much slower and less stretched than the MG/MG correlations: there is a decoupling of the motions. The behavior of the cross-correlations is rather similar to that of the MG/MG correlations. (iii) At Q-values below Q_I, dominated by inter-molecular contributions, the three partial correlation functions decay in very different ways (distinct characteristic times and β-parameters).

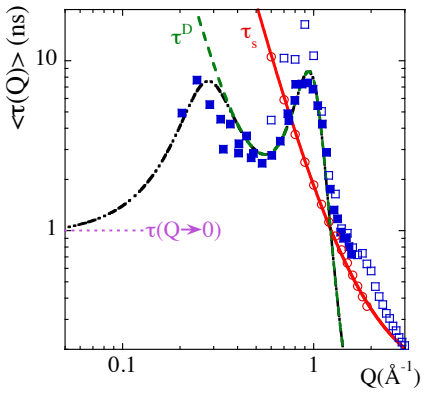

Figure 9: Momentum transfer dependence of the average characteristic time for collective (empty squares) and self-correlation (circles) functions of PIB obtained from the simulations. Filled squares are the experimental collective times.[20] Solid line: description of the self-correlation times by the anomalous jump diffusion model. Dashed-dotted line: description of the collective times by Eq. 6.[34] The dashed line represents the diffusive contribution and the horizontal dotted line indicates the location of the non-diffusive time. All data correspond to 365 K.

To understand the global behavior reflected in the total $S(Q,t)/S(Q)$ is important to consider the relative amplitudes of the partial structure factors to this function. They are presented in Figure 10(c). For Q-values below $\approx$ 1.1 Å^{-1} the dominant contribution is that of the MC/MC correlations. Therefore, the total $S(Q,t)$ behaves in a similar way to $A_{MCMC}(Q,t)$. The main difference is the slightly more stretched feature of the total function, resulting from the distinct decays of the three partial structure factors. At $Q \geq$ 1.1 Å^{-1} the relative contribution $A_{MCMC}(Q)/S(Q)$ becomes smaller than the other two in absolute value. However, in this region $A_{MCMG}(Q)/S(Q)$ nicely mirrors $A_{MGMG}(Q)/S(Q)$ and the two contributions cancel out. Therefore, the total structure factor reveals the features of the MC/MC partial correlation function regarding both, shape

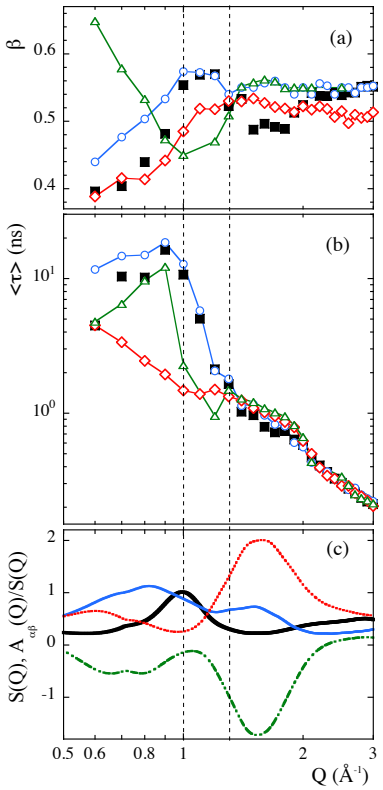

Figure 10: Momentum transfer dependence of the shape parameter (a) and average characteristic time (b) obtained from KWW fits to the total (squares) and partial correlation (circles: MC/MC, diamonds: MG/MG and triangles: MC/MG) functions of PIB at 365 K. In (c) the relative contributions of the partial structure factors to $S(Q)$ (thick line) are shown (solid: MC/MC, dotted: MG/MG and dashed-dotted: MC/MG). Vertical dotted lines mark the regions discussed in the text.

and characteristic time. We remind that, in any case, in this Q-region the three partial functions decay exactly in the same way due to the strong coupling of the intra-molecular correlations. In the Supplementary Information examples of the total and partial structure factors at different Q-values can be found.

Temperature Dependence: Origin of the $S(Q)$-Modulation of the Activation Energy

The behavior observed at the different temperatures investigated is qualitatively the same as that above described for 365 K (see Supplementary Information). However, quantitative differences develop with varying temperature that will be analyzed in the following by considering the results at the two extreme temperatures simulated. In Figure 11, the fit parameters of the partial collective correlation functions and their respective self counterparts are shown for 320 K and 470 K. Let us first discuss the results on the self-correlation functions. We observe that the value of the shape parameter for MC self-correlation hardly depends on Q and is systematically higher than that of MG self-correlations. The latter shows a sensitive Q-variation that could be attributed to the simultaneous occurrence of translational motions and methyl group rotations.[33] A gradual decoupling (separation of the characteristic times) of translational and rotational motions with decreasing temperature would explain the significant decrease of the values of the β-parameter at 320 K with respect to those at 470 K. We note however that below $Q \approx 1.5$ Å^{-1} such a decoupling hardly affects the ratio between the average times for self-motions of MCs and MGs, which is of about 2.2 at both temperatures. This implies a similar temperature dependence for both correlation times in such Q-range. The reason is that there the average relaxation time is mainly determined by the translational contribution, that would be expected to be the same for both, MC and MG subsystems and ultimately governed by the α-relaxation.

Now we focus on the emergence of collectivity in the pair-correlation functions. With exception of the β-parameter for MC/MC correlations at 320 K, all parameters of the collective functions show the feature of the corresponding partial static structure factor. In particular, we can appreciate a large influence of collective effects in the characteristic times of MC/MC correlations in the inter-molecular region. At Q_I, the ratio between collective and self characteristic times is $\langle\tau\rangle/\langle\tau_s\rangle \approx 2.3$ at 470 K. This means that correlated motions of MC units from different chains are required to achieve the structural relaxation. An important observation –as we will argue later– is that the ratio $\langle\tau\rangle/\langle\tau_s\rangle$ is increased to about 6 for 320 K. This, together with the

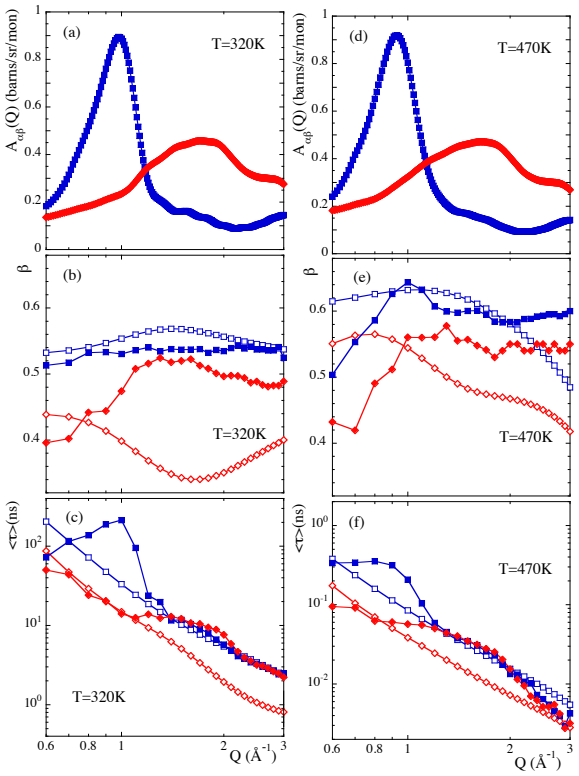

Figure 11: Momentum transfer dependence of the static partial structure factors (a,d), and the shape parameter (b,e) and average characteristic time (c,f) obtained from KWW fits to the MC/MC (filled squares) and MG/MG (filled diamonds) partial correlation functions at 320 K (left panels) and 470 K (right panels). The empty symbols represent the results of the corresponding self-correlation functions.

enhancement of stretching that takes place with decreasing temperature, suggests a growing collectivity/cooperativity of chain motion when the system approaches the glass transition. Contrarily, in the case of MG/MG correlations, the maximum ratio $\langle\tau\rangle/\langle\tau_s\rangle$ does not significantly depend on temperature.

We can thus now explain the collective effects displayed by the total dynamic structure factor (see e. g. Figure 9 for 365 K) over a such wide Q-range. In the inter-molecular length-scales region, it is caused by the strong collectivity of the dominant MC/MC correlations (high $A_{MCMC}(Q)/S(Q)$ values) that becomes more pronounced with decreasing temperature. In the intra-molecular length-

scales region, it stems from a combined effect: the collectivity of MG/MG correlations and their coupling with MC/MC motions. Both MC/MC and MG/MG correlations display the same features at such local intra-molecular length scales, which are finally those manifested by the total dynamic structure factor.

The analysis of the temperature dependence of the partial dynamic structure factors also allows identifying the origin of the modulation of the apparent activation energy of the collective times E_a with the structure factor. From the simulations in the whole temperature range investigated we have calculated E_a as function of Q for the average times of the total structure factor and the MC/MC and MG/MG partial structure factors. The results are shown in Figure 12. As can be expected from the above discussion on the relative contributions of the partial structure factors, the temperature dependence of the dynamic structure factor clearly mirrors that of the MC/MC correlations. The latter, as above mentioned, is in fact strongly determined by the increasing collectivity with decreasing temperature exhibited by the MCs in PIB. The activation energy for MG/MG correlations shows a less marked Q-dependence, displaying an average value of about 0.5 eV in the considered Q-range.

Finally, we have plotted the such obtained values of E_a for the total dynamic structure factor (free β-parameter, whole T-range investigated) as empty squares in Figure 2. Using a varying β-parameter influences most the low-Q results, leading to a smoother Q-dependence of the apparent activation energy.

ANALYTICAL MODEL FOR THE COLLECTIVE RESPONSE AT MESOSCALES

In a recent work[34] we successfully described the Q-dependence of the experimentally determined collective characteristic time of PIB[20] in the whole Q-range covered in those experiments, $0.2 \leq Q \leq 1.8$ Å^{-1}. This range includes the neighborhood of the structure factor peak and the so-called intermediate length scales regime. As an example, Figure 9 shows the case of the results

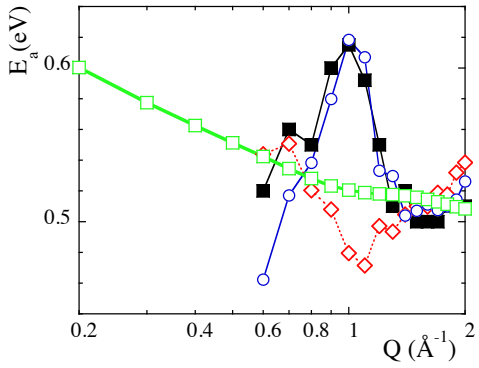

Figure 12: Momentum transfer dependence of the apparent activation energy of the average characteristic time for collective relaxation obtained from the simulations for the total dynamic structure factor (filled squares) and for the partial structure factors: MC/MC (circles) and MG/MG (diamonds). Empty squares show the Q-dependence of E_a^s. In all cases Q- and T-dependent β-values and the whole investigated T-range have been considered in the determination of the activation energy.

at 365 K (filled squares) and their description (dashed-dotted line). The model used consists of an interpolation formula that embeds the mesoscopic (non-diffusive) and the high-Q (diffusive) limits of the collective times in an analytical expression as proposed by Novikov et al.:[35]

$$\frac{1}{\tau(Q)} = \frac{1}{\tau(Q \to 0)} e^{-Q^2 \xi_c^2} + \frac{1}{\tau^D(Q)}. \tag{6}$$

The non-diffusive (Q-independent) time should reflect the viscoelastic coupling of stress and density fluctuations on scales long enough compared to atomic dimensions, but not yet in the hydro-

dynamic limit.[35] Its contribution to the total collective time is affected by a Gaussian cutoff factor $e^{-Q^2\xi_c^2}$ to ensure that it is present only on length scales beyond a characteristic length ξ_c, which is assumed to be $\xi_c \sim 2\pi/Q_I$. To model the diffusive time $\tau^D(Q)$, we generalized the expression given in Ref.[35] to the case of sublinear diffusion. Then the self-correlation time $\tau_s(Q)$ can be expressed by the anomalous jump diffusion model:[59]

$$\tau_s(Q) \;=\; \tau_o \left[1 + \frac{1}{Q^2\ell_o^2}\right]^{\frac{1}{\beta_s}}, \tag{7}$$

which assumes that the resulting sublinear increase of the mean squared atomic displacement $\langle r^2(t)\rangle \;\propto\; t^{\beta_s}$ has its origin in a distribution of elementary jumps. Here ℓ_o is the preferred jump distance and τ_o the time between jumps. As can be seen in Figure 9, Eq. 7 describes nicely the average self-characteristic times of PIB determined from the simulations. A temperature-independent value of 0.6 Å is obtained for ℓ_o. In the spirit of a Sköld[60]-like renormalization, the collective diffusive counterpart can be expressed as:[34]

$$\tau^D(Q) \;=\; S(Q)^{\frac{1}{\beta_s}}\tau_o \left[1 + \frac{1}{Q^2\ell_o^2}\right]^{\frac{1}{\beta_s}} \tag{8}$$

As can be seen in Figure 9, the prediction of Eq. 8 (dashed line) describes rather well the collective times in the neighborhood of Q_I. Considering also a non-diffusive contribution (depicted as the horizontal dotted line in Figure 9) the full model expressed by Eq. 6 (dashed-dotted line) reproduces vey nicely the experimentally observed behavior.

In Ref.[34] it was also shown that the model gave account for the Q-dependence of the activation energy for collective times (see dashed-dotted line in Figure 2), in particular for its modulation by the structure factor in the neighborhood of its first maximum. We also note the excellent agreement with the results when a variable β-value is considered to describe the collective data (empty squares). The question arises: to which extent is this modulation a consequence of the combination of the two relaxation mechanisms? As can be realized in Figure 9, due to the cutoff function employed, the non-diffusive contribution would be appreciable only at Q-values below and around

0.4 Å^{-1}. Consequently, in the range $Q \geq 0.4$ Å^{-1} the activation energy should be fully determined by the temperature dependence of τ_D. Following Eq. 8, given a pair of temperatures T_1 and T_2, the apparent activation energy of τ_D (E_a^D) should be related to that of the elementary self-correlation times τ_o (E_a^s) via the expression:

$$E_a^D = E_a^s + \frac{k_B}{\left(\frac{1}{T_1} - \frac{1}{T_2}\right)} \ln \left(\frac{\left[S(Q,T_1)\left(1+\frac{1}{Q^2\ell_o(T_1)^2}\right)\right]^{\frac{1}{\beta_s(T_1)}}}{\left[S(Q,T_2)\left(1+\frac{1}{Q^2\ell_o(T_2)^2}\right)\right]^{\frac{1}{\beta_s(T_2)}}} \right). \quad (9)$$

Considering the extreme temperatures experimentally explored (335 and 390 K), we have calculated the result of Eq. 9 by using the simulated data. In this range E_a^s = 0.54 eV, and the values of the β_s-exponents are 0.44 (335 K) and 0.49 (390 K) (see Supplementary Information). The obtained curve is represented in Figure 2 as a dashed line. It nicely reproduces the maximum of the activation energy around Q_I. Interestingly enough, from inspection of Eq. 9 we deduce that this modulation is just a consequence of the temperature dependence of the static structure factor. Thus, the observed effect is accounted for by the Sköld-like renormalized function, even if this phenomenological approach does not imply a knowledge of the relevant partial contributions to the dynamic structure factors in this Q-region.

Last, we also comment on the increase of E_a^D with decreasing Q below $Q \approx 0.4$ Å^{-1} –where $S(Q)$ does not depend on Q.[20] This tendency reflects an increase of the activation energy of the self-motions E_a^s (see empty symbols in Figure 12). The increase of E_a^s with decreasing Q is a consequence of the decrease of the value of β_s with decreasing temperature. In the low-Q range the behavior is close to Gaussian and consequently the characteristic time follows a power law in Q as Q^{-2/β_s}.[61] Since β_s decreases with decreasing temperature, the activation energy increases with decreasing Q. A similar observation has recently been reported for polyethylene-like chains.[62] In that work, it was attributed to an intimate link between local dynamics and long-range motion. We may speculate that this could also be case for PIB, where methyl-group dynamics and translational motions seem to be highly coupled. In any case, the non-diffusive component in Eq. 6 prevents the up-turn of the resulting E_a with decreasing Q and the activation energy for collective motion is

predicted to decrease again at intermediate length scales (see Figure 2).

CONCLUDING REMARKS

Our properly validated simulations have allowed unravelling the dynamic and structural details of PIB at length scales in the inter- and intra-molecular range. Remarkable results when unveiling the origin of the structure factor are (i) the attribution of the variations of the first peak with temperature to mainly the evolution of the cross-correlations involving main-chain and methyl group atoms. The increase of the intensity in the peak and lower Q-values with increasing temperature is a consequence of the homogeneization of the local density fluctuations. (ii) Paradoxically, in the position of the actual peak relating methyl group / methyl group correlations a marked minimum appears in the structure factor. This is a consequence of the strong negative cross-correlations in this region. Furthermore, we have been able to determine the Q-ranges of the static structure factor where either inter- or intra-molecular correlations are dominant.

Regarding the dynamics, we have found that in PIB the decay of the intra-molecular correlations takes place through highly coupled motions relating pairs of methyl groups and methyl groups and backbone atoms along the same chain. The correlated character of the intra-molecular dynamics persists in the whole temperature range here investigated. A coupling mechanism between methyl rotation and a fast relaxation motion associated with the chain backbone was already proposed in a study of PIB methyl dynamics combining MD-simulations and ^{13}NMR experiments[33] and suggested as a possible explanation of the discrepancies between the outcomes of the analysis of collective and self-motions by neutron scattering.[14]

The relaxation of the inter-molecular correlations between backbones occurs also in a collective way –at inter-molecular length scales, the decay of the self-correlations of main-chain atoms is much faster than that of their pair correlations. As the system approaches the glass-transition, the collectivity of MC/MC correlations is gradually enhanced. This collectivity of the backbones is ultimately the responsible for the modulation of the activation energy with the structure factor

found in the experiments[20] and reproduced by our simulations. In other words, the above mentioned tendency to homogenize the local density fluctuations at high temperature is accompanied by a release of the collectivity of backbone motions.

Collectivity of MC/MC correlations at the first structure factor peak has also been found in other polymers previously investigated following a similar approach like poly(methyl methacrylate) (PMMA),[63] poly(vinyl acetate) (PVAc)[7] and poly(ethylene propylene) (PEP).[56] We note the strong similarities of the behavior at inter-molecular level of PIB and PEP. In addition, PEP also displays an activation energy for collective relaxation that mirrors the static structure factor. On the contrary, the large collectivity exhibited by the dynamics at intra-molecular level of PIB is clearly not present in the above mentioned polymers. In all those systems, the side-groups intra-molecular correlations relax in the same way as their respective self-correlations, revealing complete loss of collectivity and thus independent motions. Only for PMMA the MC/MC correlations show still some degree of collectivity at such short length scales.

Last, we have analyzed the components of the recently proposed ansatz based on Sköld's approximation and the anomalous jump diffusion model to describe the collective response of PIB. The modulation of the apparent activation energy reproduced by this approach stems only from the diffusive contribution and is a mere consequence of the variation of the structure factor with temperature. From the above discussion, it follows that this evolution is what ultimately determines collectivity effects. To give account for the collective behavior at lower Q-values, in the intermediate length scales regime, an additional ingredient is needed; the non-diffusive relaxation mechanism recently proposed in Refs.[34,35] seems to be a plausible candidate.

Acknowledgements

Y. K. acknowledges the grant of the Spanish Ministry. We thank support from the projects IT-654-13 (GV) and MAT2012-31088.

Supplemetary information is available free of charge via the Internet at http://pubs.acs.org/.

References

References

(1) Frick, B.; Richter, D.; Ritter, C. *Europhys. Lett.* **1989**, *9*, 557.

(2) Richter, D.; Frick, B.; Farago, B. *Phys. Rev. Lett.* **1988**, *61*, 2465.

(3) Arbe, A.; Richter, D.; Colmenero, J.; Farago, B. *Phys. Rev. E* **1996**, *54*, 3853.

(4) Ayyagari, C.; Bedrov, D.; Smith, G. D. *Macromolecules* **2000**, *33*, 6194.

(5) Colmenero, J.; Alvarez, F.; Arbe, A. *Phys. Rev. E* **2002**, *65*, 041804.

(6) Genix, A.-C.; Arbe, A.; Alvarez, F.; Colmenero, J.; Schweika, W.; Richter, D. *Macromolecules* **2006**, *39*, 3947.

(7) Tyagi, M.; Arbe, A.; Alvarez, F.; Colmenero, J.; Gonzalez, M. A. *J. Chem. Phys.* **2008**, *129*, 224903.

(8) Slichter, W. P. *J. Polym. Sci.: Part C* **1966**, *14*, 33.

(9) Törmälä, P. *J. Macromol. Sci.–Rev. Macromol. Chem. C* **1979**, *17*, 297.

(10) Dejean de la Batie, R.; Lauprtre, F.; Monnerie, L. *Macromolecules* **1989**, *22*, 2617–2622.

(11) Kunal, K.; Paluch, M.; Roland, C. M.; Puskas, J. E.; Chen, Y.; Sokolov, A. P. *Journal of Polymer Science Part B: Polymer Physics* **2008**, *46*, 1390–1399.

(12) Frick, B.; Richter, D.; Trevino, S. *Physica A* **1993**, *201*, 88–94.

(13) Frick, B.; Richter, D. *Physical Review B* **1993**, *47*, 14795.

(14) Arbe, A.; Colmenero, J.; Frick, B.; Monkenbusch, M.; Richter, D. *Macromolecules* **1998**, *31*, 4926–4934.

(15) Richter, D.; Arbe, A.; Colmenero, J.; Monkenbusch, M.; Farago, B.; Faust, R. *Macromolecules* **1998**, *31*, 1133–1143.

(16) Londono, J. D.; Habenschuss, A.; Curro, J. G.; Rajasekaran, J. J. *Journal of Polymer Science Part B: Polymer Physics* **1996**, *34*, 3055–3061.

(17) Richter, D.; Monkenbusch, M.; Allgaier, J.; Arbe, A.; Colmenero, J.; Farago, B.; Cheol Bae, Y.; Faust, R. *J. Chem. Phys.* **1999**, *111*, 6107.

(18) Kanaya, T.; Kawaguchi, T.; Kaji, K. *Macromolecules* **1999**, *32*, 1672–1678.

(19) Kisliuk, A.; Mathers, R. T.; Sokolov, A. P. *J. Polym. Sci.: Part B: Polym. Physics* **2000**, *38*, 2785.

(20) Farago, B.; Arbe, A.; Colmenero, J.; Faust, R.; Buchenau, U.; Richter, D. *Phys. Rev. E* **2002**, *65*, 051803.

(21) Triolo, A.; Lechner, R. E.; Desmedt, A.; Telling, M. T. F.; Arrighi, V. *Macromolecules* **2002**, *35*, 7039–7043.

(22) Arrighi, V.; Triolo, A.; Qian, H. *Journal of Non-Crystalline Solids* **2002**, *307-310*, 654–657.

(23) Ganazzoli, F.; Raffaini, G.; Arrighi, V. *Physical Chemistry Chemical Physics* **2002**, *4*, 3734–3742.

(24) Ding, Y.; Novikov, V. N.; Sokolov, A. P.; ; Dalle-Ferrier, C.; Alba-Simionesco, C.; Frick, B. *Macromolecules* **2004**, *37*, 9264–9272.

(25) Adams, M. A.; Gabrys, B. J.; Zajac, W. M.; Peiffer, D. G. *Macromolecules* **2005**, *38*, 160–166.

(26) Begen, B.; Kisliuk, A.; Novikov, V.; Sokolov, A.; Niss, K.; Chauty-Cailliaux, A.; Alba-Simionesco, C.; Frick, B. *J. of Non-Cryst. Solids* **2006**, *42-49*, 4583 – 4588.

(27) Niss, K.; Begen, B.; Frick, B.; Ollivier, J.; Beraud, A.; Sokolov, A.; Novikov, V. N.; Alba-Simionesco, C. *Phys. Rev. Lett.* **2007**, *99*, 055502.

(28) Niss, K.; Dalle-Ferrier, C.; Giordano, V. M.; Monaco, G.; Frick, B.; Alba-Simionesco, C. *The Journal of Chemical Physics* **2008**, *129*, –.

(29) Dalle-Ferrier, C.; Niss, K.; Sokolov, A. P.; Frick, B.; Serrano, J.; Alba-Simionesco, C. *Macromolecules* **2010**, *43*, 8977–8984.

(30) Arbe, A.; Alvarez, F.; Colmenero, J. *Soft Matter* **2012**, *8*, 8257–8270.

(31) Karatasos, K.; Ryckaert, J.-P. *Macromolecules* **2001**, *34*, 7232–7235.

(32) Karatasos, K.; Saija, F.; Ryckaert, J.-P. *Physica B* **2001**, *301*, 119–125.

(33) Karatasos, K.; Ryckaert, J.-P.; Ricciardi, R.; Laupretre, *Macromolecules* **2002**, *35*, 1451–1462.

(34) Colmenero, J.; Alvarez, F.; Khairy, Y.; Arbe, A. *J. Chem. Phys.* **2013**, *139*, 044906.

(35) Novikov, V. N.; Schweizer, K. S.; Sokolov, A. P. *J. Chem. Phys.* **2013**, *138*, 164508.

(36) *www.accelrys.com*

(37) Bunte, S. W.; Sun, H. *J. Phys. Chem. B* **2000**, *104*, 2477.

(38) Sun, H. *J. Phys. Chem. B* **1998**, *102*, 7338.

(39) Yang, J.; Ren, Y.; Tian, A.; Sun, H. *J. Phys. Chem. B* **2000**, *104*, 4951.

(40) Theodorou, D.; Suter, U. *Macromolecules* **1986**, *19*, 139.

(41) Theodorou, D.; Suter, U. *Macromolecules* **1986**, *19*, 379.

(42) Kotelyanski, M., Theodorou, D., Eds. *Simulation Methods for Polymers*; Marcel Dekker: New York, 2004.

(43) Fetters, L. J.; Lohse, D. J.; Richter, D.; Witten, T. A.; Zirkel, A. *Macromolecules* **1994**, *27*, 4639.

(44) Mark, J. E. *Physical Properties of Polymers Handbook*; AIP Press, New York, 1996.

(45) Lovesey, S. W. *Theory of Neutron Scattering from Condensed Matter*; Clarendon Press, Oxford, 1984.

(46) Mezei, F. *Neutron Spin Echo, Lecture Notes in Physics, Vol. 28*; Springer-Verlag, Heidelberg, 1980.

(47) Narros, A.; Alvarez, F.; Arbe, A.; Colmenero, J.; Richter, D.; Farago, B. *J. Chem. Phys.* **2004**, *121*, 3282.

(48) Cho, D.; Neuburger, N.; Mattice, W. L. *Macromolecules* **1992**, *25*, 322.

(49) Madkour, T. M.; Mohammed, O. I.; Ebaid, A. E. *J. of Macromolecular Science, Part B: Physics* **2000**, *39(5&6)*, 679.

(50) DeBolt, L. C.; Suter, U. W. *Macromolecules* **1987**, *20*, 1425.

(51) Fetters, L. J.; Lohse, D. J.; Richter, D.; Witten, T. A.; Zirkel, A. *Macromolecules* **1994**, *27*, 4639.

(52) Press, W. *J. Chem. Phys* **1972**, *56*, 2597.

(53) Tsolou, G.; Mavrantzas, V. G.; Makrodimitri, Z. A.; Economou, I. G.; Gani, R. *Macromolecules* **2008**, *41*, 6228–6238.

(54) Gerstl, C.; Brodeck, M.; Schneider, G. J.; Su, Y.; Allgaier, J.; Arbe, A.; Colmenero, J.; Richter, D. *Macromolecules* **2012**, *45*, 7293.

(55) Moreno, A.; Arbe, A.; Colmenero, J. *Macromolecules* **2011**, *44*, 1695.

(56) Pérez-Aparicio, R.; Arbe, A.; Alvarez, F.; Colmenero, J.; Willner, L. *Macromolecules* **2009**, *42*, 8271.

(57) Busselez, R.; Arbe, A.; Alvarez, F.; Colmenero, J.; Frick, B. *J. Chem. Phys.* **2011**, *134*, 054904.

(58) Smith, G. D.; Bedrov, D.; Paul, W. *J. Chem. Phys.* **2004**, *121*, 4961.

(59) Arbe, A.; Colmenero, J.; Alvarez, F.; Monkenbusch, M.; Richter, D.; Farago, B.; Frick, B. *Phys. Rev. E* **2003**, *67*, 051802.

(60) Sköld, K. *Phys. Rev. Lett.* **1967**, *19*, 1023.

(61) Colmenero, J.; Alegría, A.; Arbe, A.; Frick, B. *Phys. Rev. Lett.* **1992**, *69*, 478.

(62) Arrighi, V.; Tanchawanich, J.; Telling, M. T. F. *Macromolecules* **2013**, *46*, 216–225.

(63) Genix, A.-C.; Arbe, A.; Alvarez, F.; Colmenero, J.; Farago, B.; Wischnewski, A.; Richter, D. *Macromolecules* **2006**, *39*, 6260.

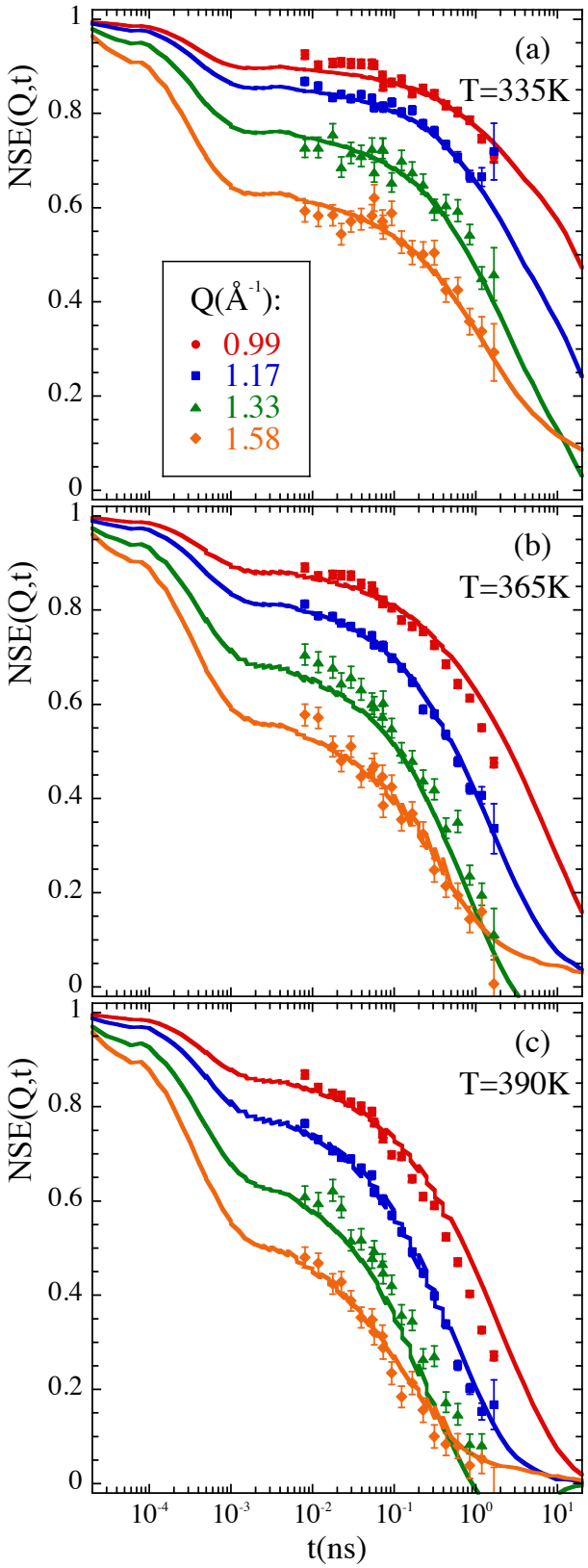
(a)
T=335K
(b)
T=365K
(c)
T=390K
NSE(Q,t)
Q(Å^{-1}):
0.99
1.17
1.33
1.58
t(ns)

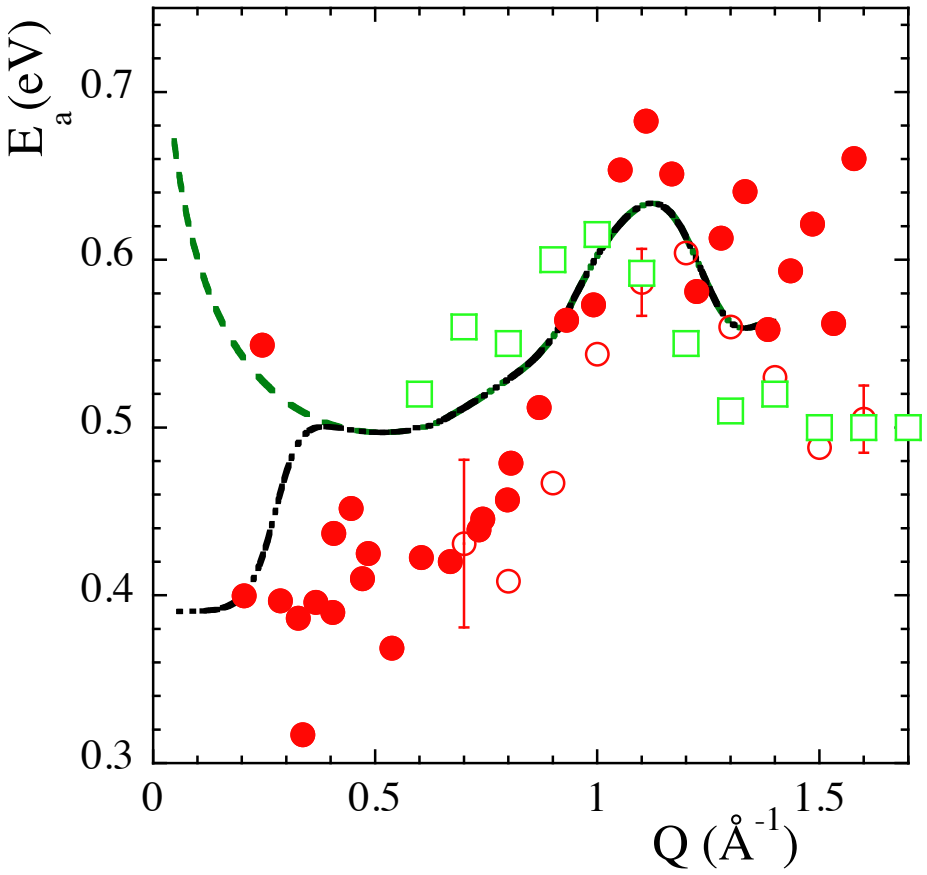
E a (eV)
0.7
0.6
0.5
0.4
0.3
0
0.5
1
1.5
Q (Å-1)

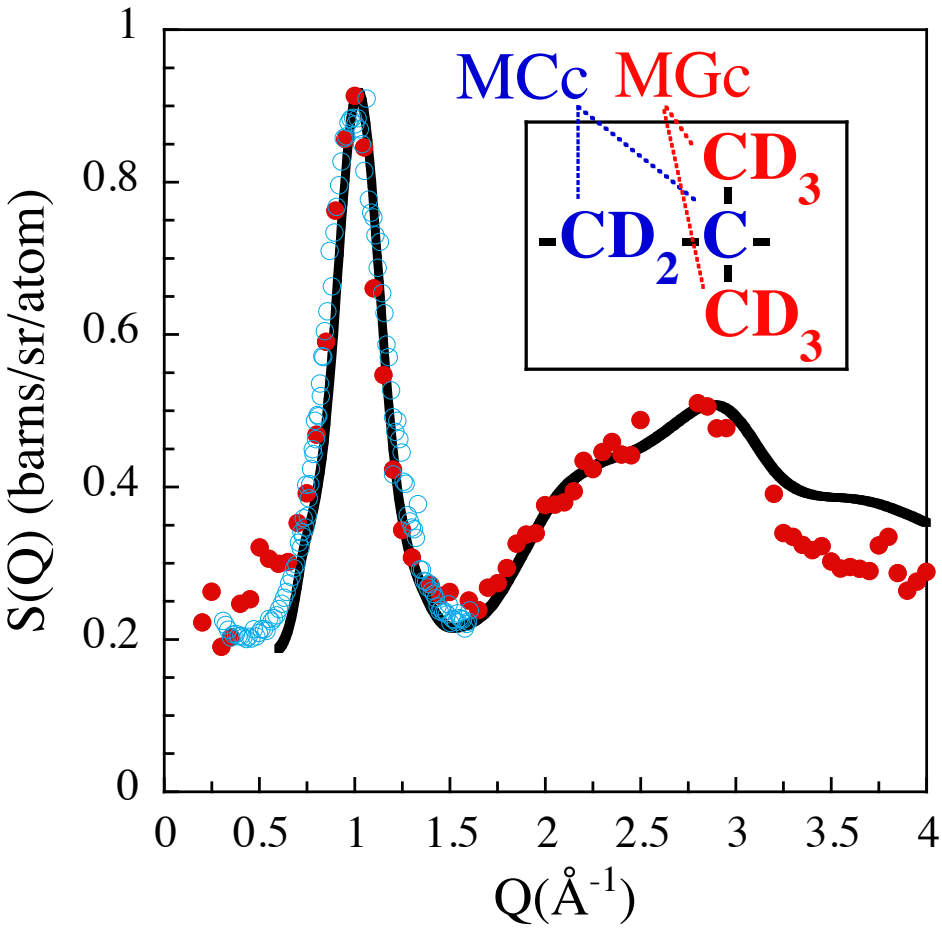
MCc
MGc
CD3
-CD2-C-
CD3
S(Q) (barns/sr/atom)
Q(Å-1)
0
0.2
0.4
0.6
0.8
1
0
0.5
1
1.5
2
2.5
3
3.5
4

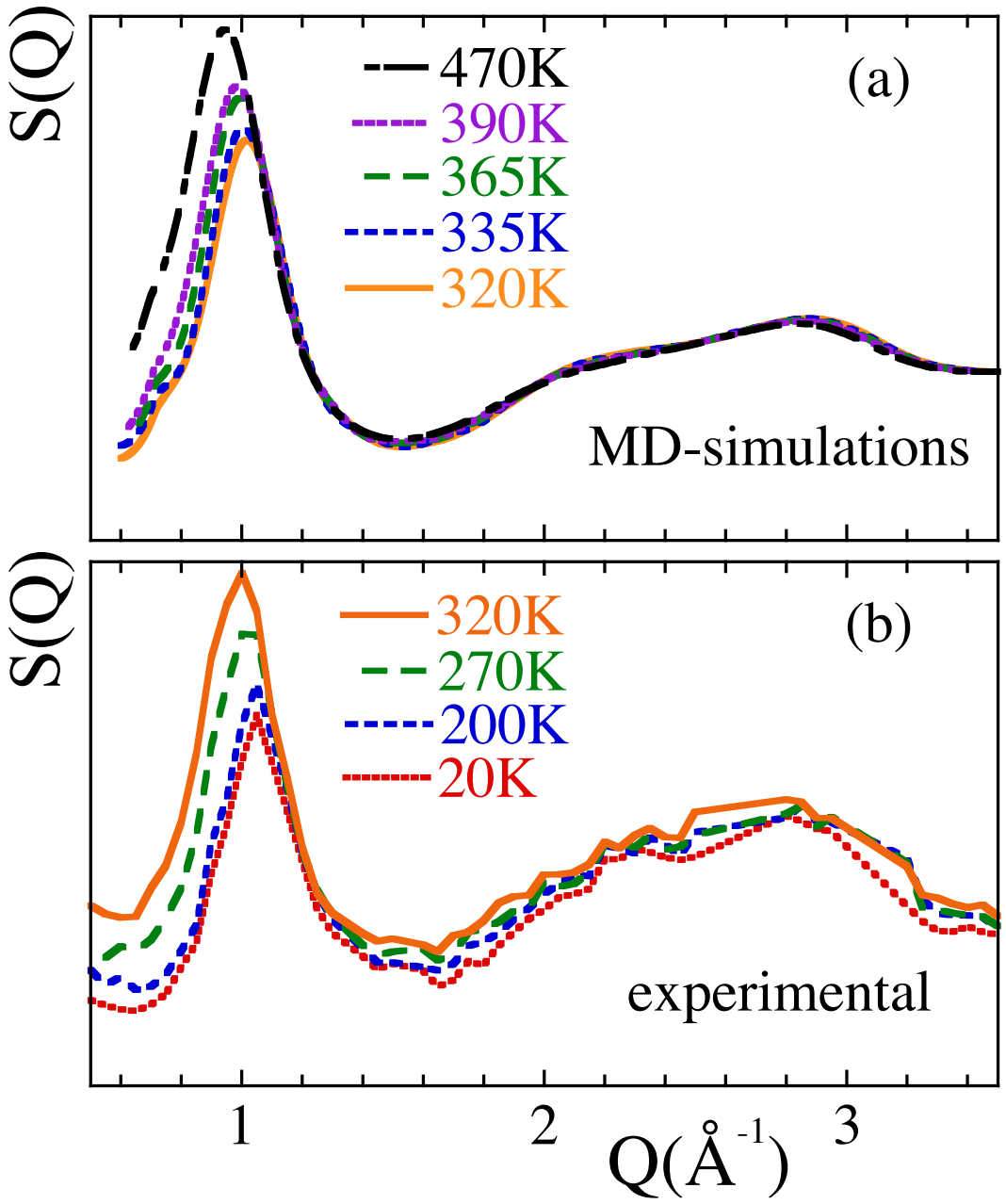
S(Q)
470K
390K
365K
335K
320K
(a)
MD-simulations
S(Q)
320K
270K
200K
20K
(b)
experimental
1
2
3
Q(Å-1)

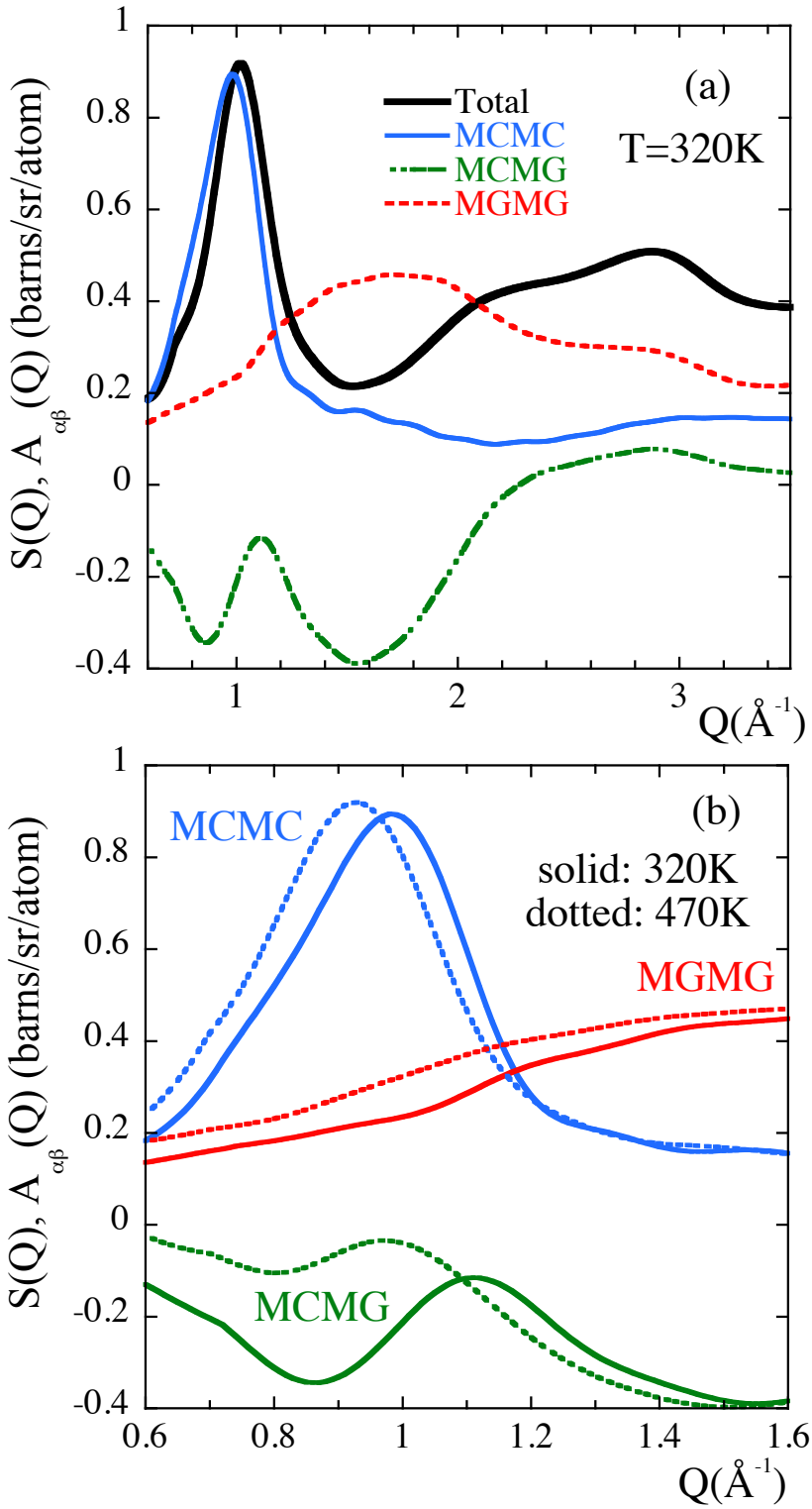
(a)
T=320K
Total
MCMC
MCMG
MGMG
S(Q), A αβ (Q) (barns/sr/atom)
Q(Å-1)
(b)
solid: 320K
dotted: 470K
MCMC
MGMG
MCMG
S(Q), A αβ (Q) (barns/sr/atom)
Q(Å-1)

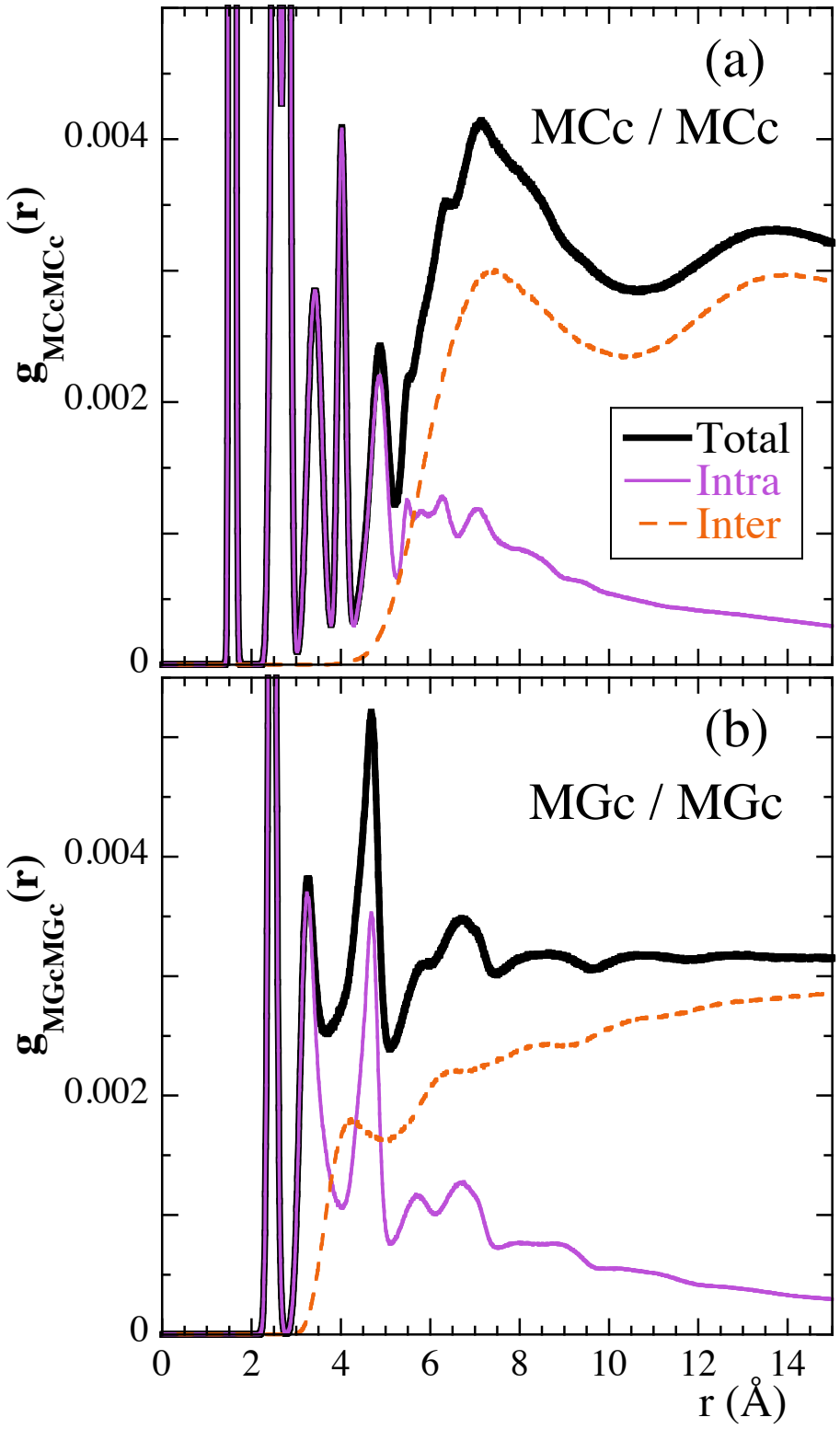
(a)
MCc / MCc
0.004
0.002
0
$g_{MCcMCc}(r)$
Total
Intra
Inter
(b)
MGc / MGc
0.004
0.002
0
$g_{MGcMGc}(r)$
0
2
4
6
8
10
12
14
r (Å)

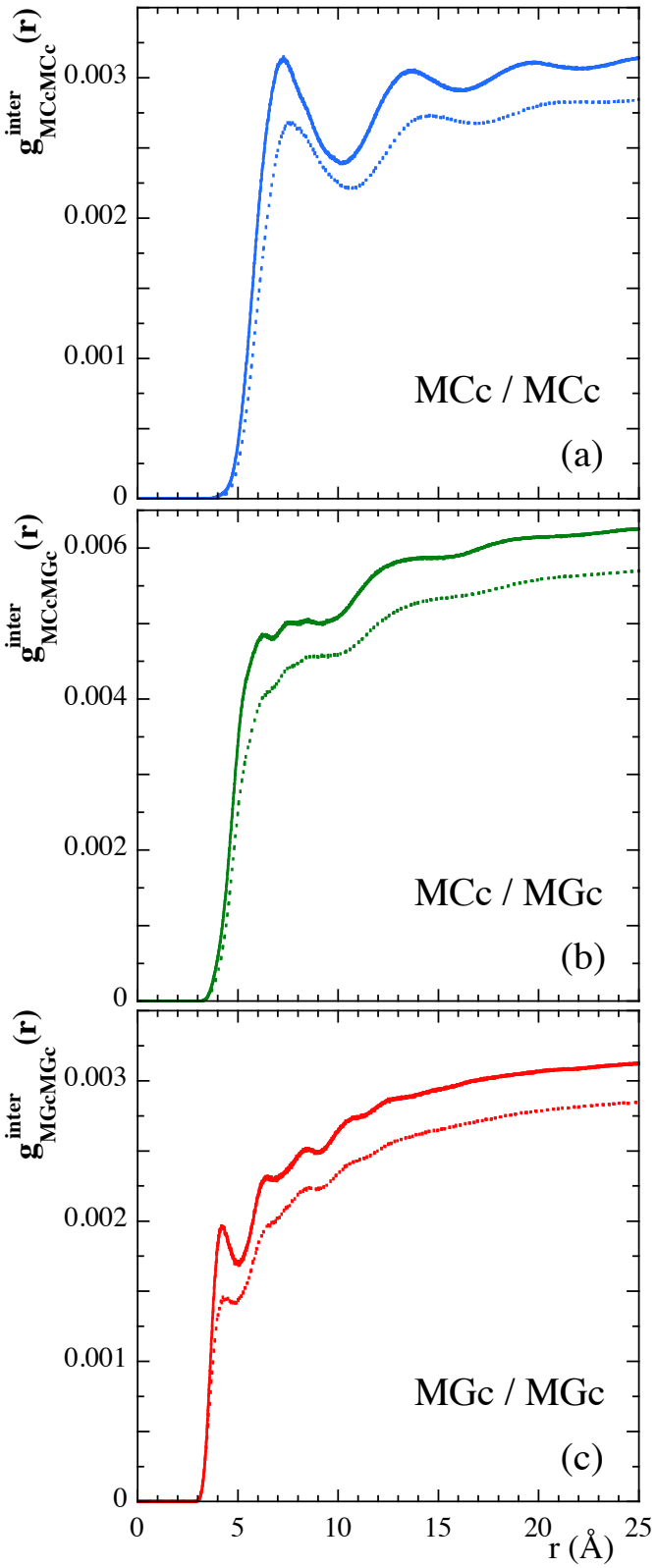
$g^{inter}_{MCcMCc}(r)$
0.003
0.002
0.001
0
MCc / MCc
(a)
$g^{inter}_{MCcMGc}(r)$
0.006
0.004
0.002
0
MCc / MGc
(b)
$g^{inter}_{MGcMGc}(r)$
0.003
0.002
0.001
0
MGc / MGc
(c)
0
5
10
15
20
25
r (Å)

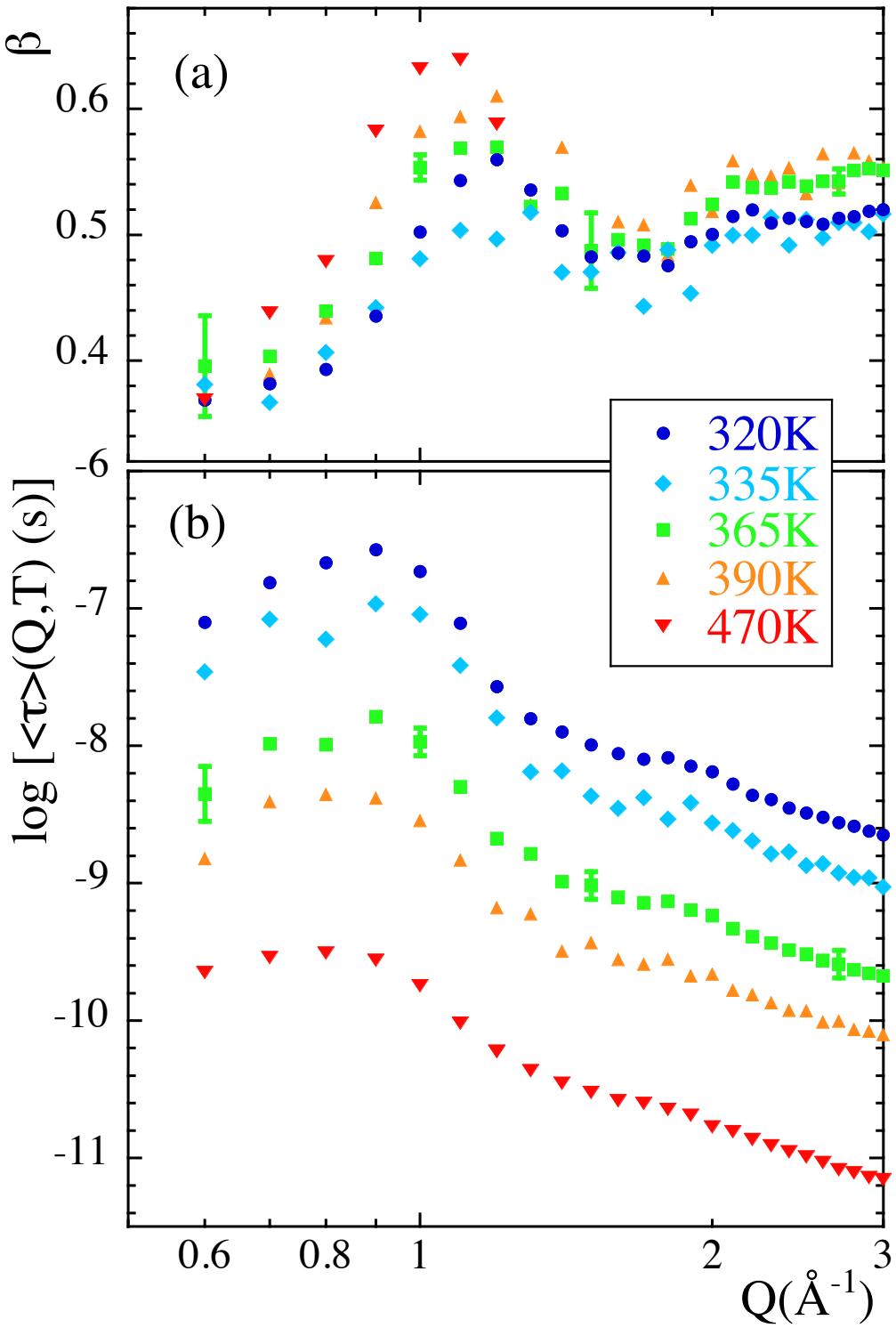
β
(a)
0.6
0.5
0.4
320K
335K
365K
390K
470K
(b)
log [<τ>(Q,T) (s)]
-6
-7
-8
-9
-10
-11
0.6
0.8
1
2
3
Q(Å-1)

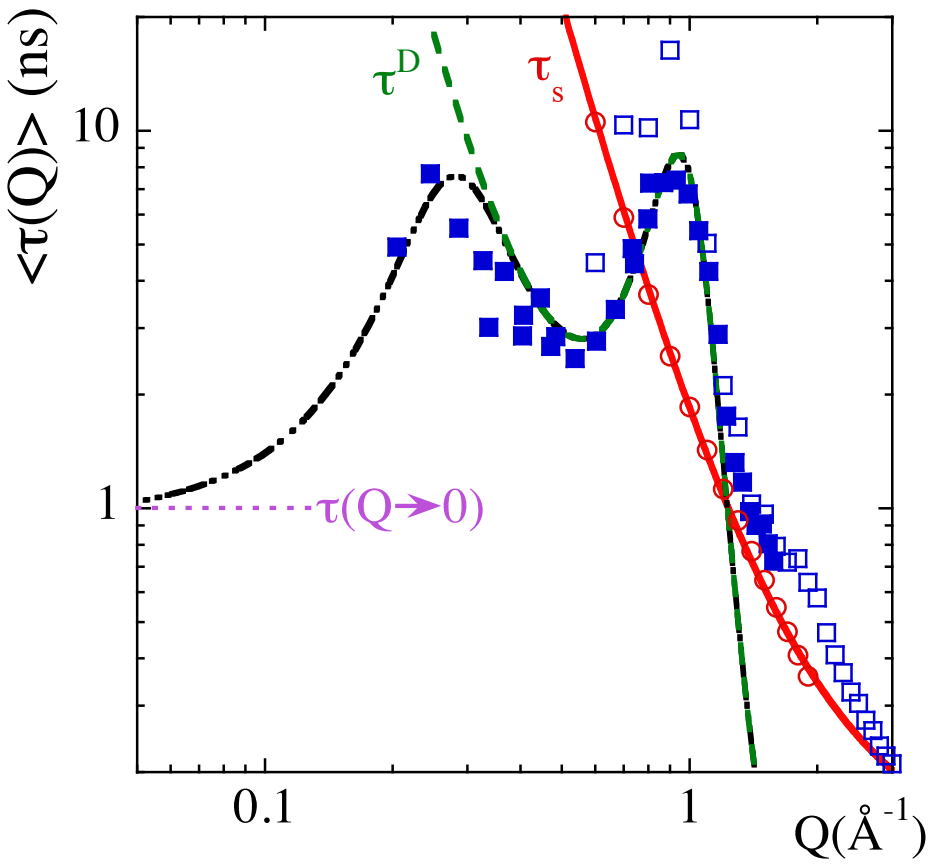
τ^D
τ_s
$\tau(Q\rightarrow 0)$
10
1
0.1
1
Q(Å^{-1})
<τ(Q)> (ns)

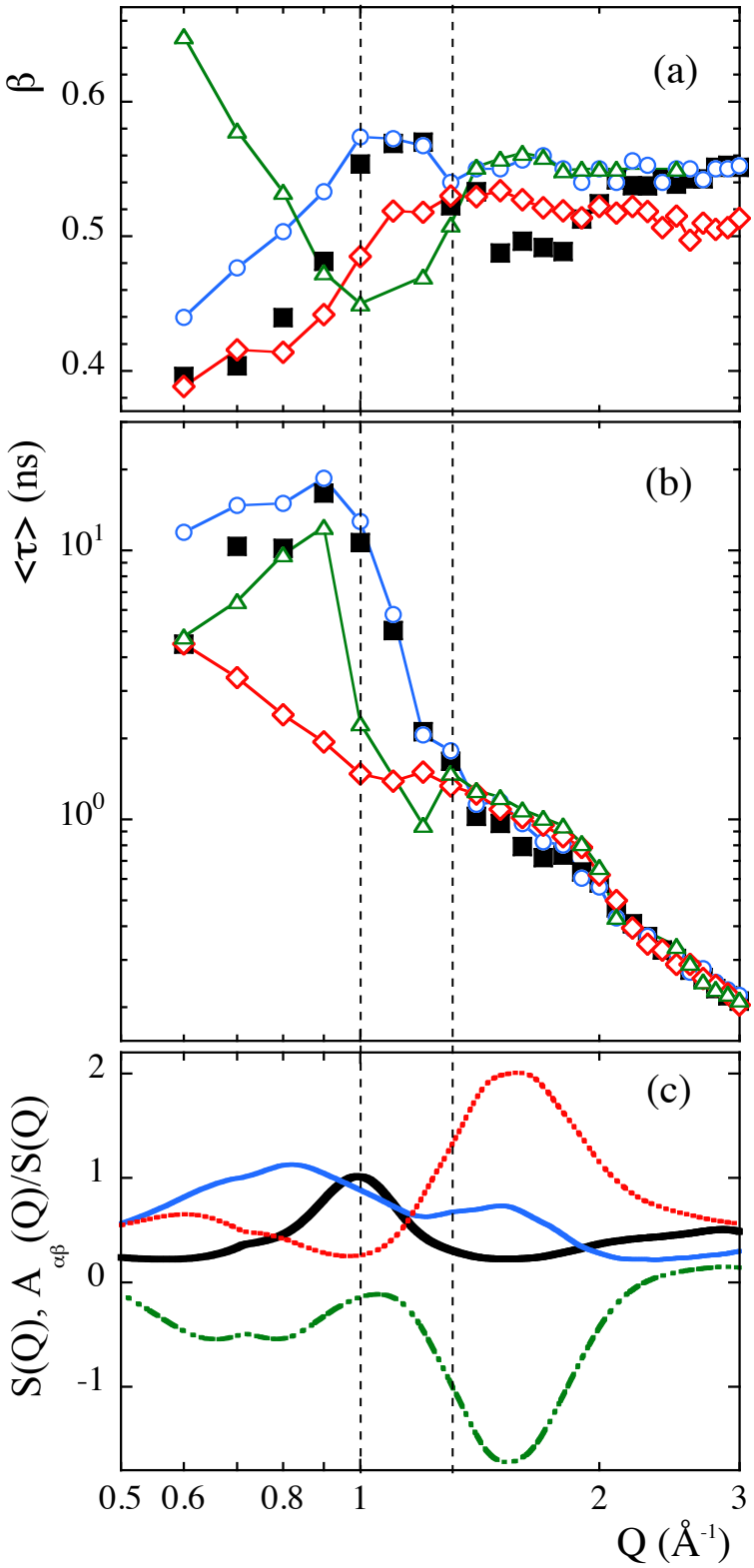
(a)
β
0.6
0.5
0.4
(b)
<τ> (ns)
10^1
10^0
(c)
S(Q), A_αβ (Q)/S(Q)
2
1
0
-1
0.5
0.6
0.8
1
2
3
Q (Å^-1)

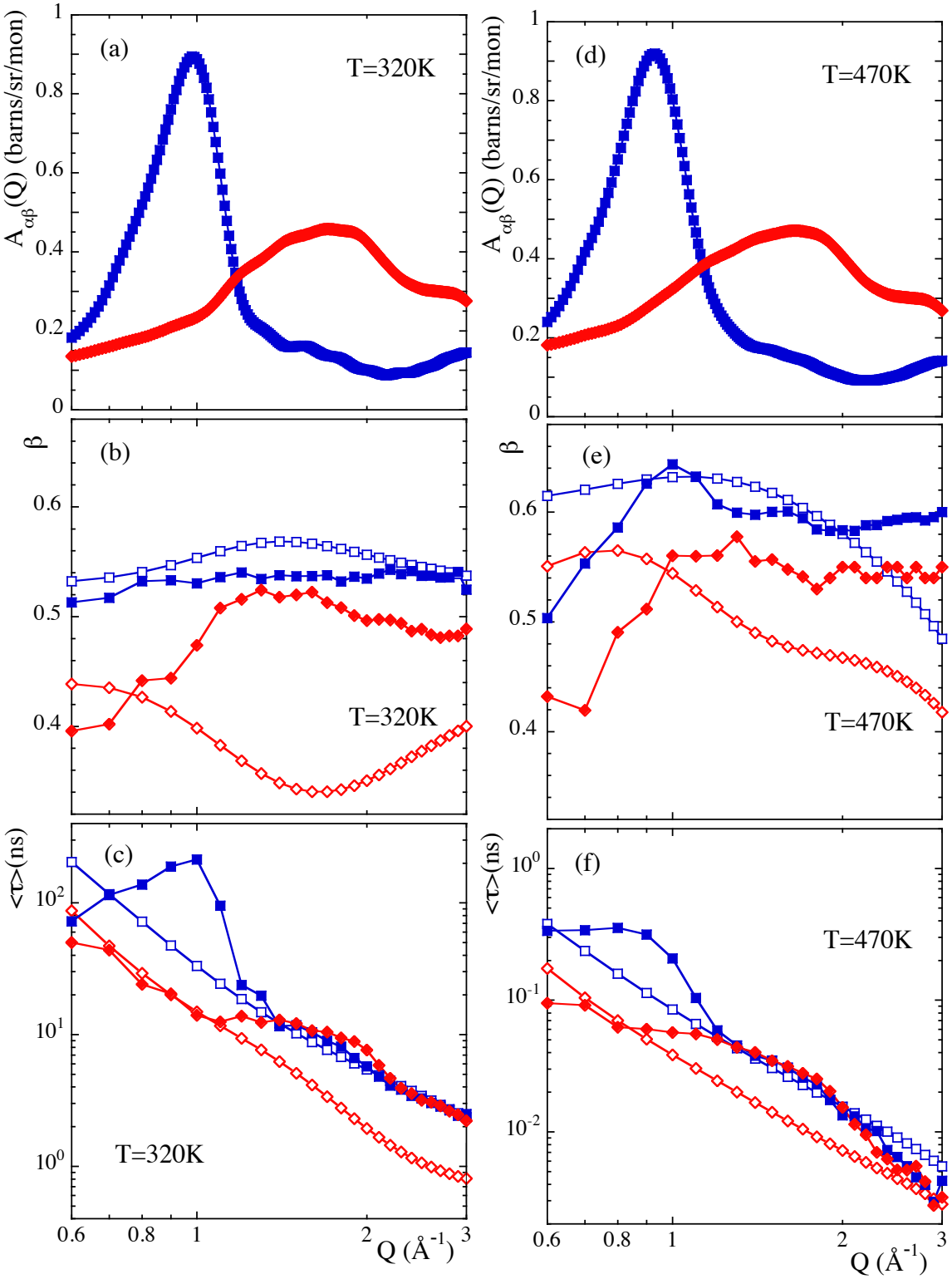
(a)
T=320K
$A_{\alpha\beta}(Q)$ (barns/sr/mon)
(b)
β
T=320K
(c)
<τ>(ns)
T=320K
Q (Å^{-1})
(d)
T=470K
$A_{\alpha\beta}(Q)$ (barns/sr/mon)
(e)
β
T=470K
(f)
<τ>(ns)
T=470K
Q (Å^{-1})

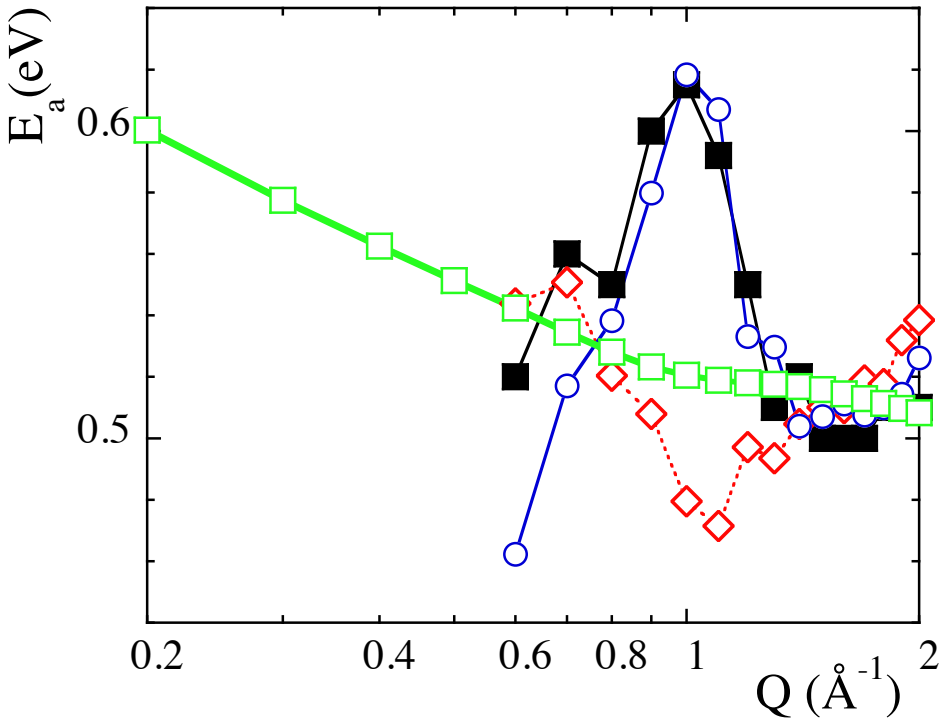
E_a (eV)
0.6
0.5
0.2
0.4
0.6
0.8
1
2
Q (Å^-1)

FOR TABLE OF CONTENTS USE ONLY

'Collective Features in Polyisobutylene. A Study of the Static and Dynamic Structure Factor by Molecular Dynamics Simulations'

Y. Khairy, F. Alvarez, A. Arbe and J. Colmenero